Author response to interactive comment on "Henry, A. C. J., Drews, R., Schannwell, C., and Višnjević, V.: Hysteretic evolution of ice rises and ice rumples in response to variations in sea level, EGUsphere [preprint], https://doi.org/10.5194/egusphere-2022-128, 2022."

We would like to thank the referees for the positive and thorough review of our paper. We appreciate the time taken and welcome your helpful comments. We have revised the manuscript to address your review comments (see below). Our replies are written in bold font.

1 Reply to Anonymous Referee #1

General comments

The paper 'Hysteretic evolution of ice rises and ice rumples in response to variations in sea level' by Clara Henry, Reinhard Drews, Clemens Schannwell and Vjeran Višnjevic is a modeling study making use of the Finite Element code Elmer/Ice in order to investigate, from synthetic three-dimensional scenarios, the stability of ice rises and ice rumples, as well as the dynamical transition from one flow regime to the other depending on the amount of friction at the ice/bed interface. To this end, starting from an initial steady state corresponding to an ice rise situation, perturbation experiments consisting in cycles of sea level rise and decrease are run solving the full-Stokes set of equations. Obtained initial steady surface velocities on the grounded part are compared to their Shallow Ice Approximation (SIA) counterparts in order to quantify the importance of longitudinal stresses transmitted from the surrounding ice shelf to the grounded ice. Unsurprisingly deviations are significant when basal friction is low, whereas they become negligible in the high basal friction scenario. The transient simulations show that an increase of sea-level induces a transition from an ice rise flow regime to an ice rumple regime in all friction scenarios. However, in the high friction scenario, much higher sea level increase is required than in the other scenarios to switch from the ice rise to the ice rumple regime, and the latter is unstable (i.e. complete ungrounding rapidly occurs). Interestingly, the sea level decrease experiments bring to light a hysteretic response of grounded ice, with the grounded area and induced buttressing effect being systematically lower than in the sea level increase phases when sea level is decreased back to its initial level. Conclusions are then drawn regarding the initialisation of ice flow models as well as the inversion of basal friction parameters.

Overall, the paper is well-written, the proposed methodology is rigorous, the experiments are well-designed, the figures are mostly clear and relevant, the supplementary video is very illustrative, and the conclusions regarding the stability of ice rises, as well as the highlighted hysteretic behavior in response to sea-level changes and associated irreversibility are significant for improvement of the accuracy of sea level rise projections. Therefore, I think the paper ought to be published and I have only a few minor modifications/comments to propose.

Response: Thank you for your comments which have resulted in a clearer presentation of our results. We have addressed the concerns regarding the grounding line implementation by running equivalent simulations using the "Discontinuous" and "Last Grounded" definitions, which show that the hysteretic behaviour also occurs for the other grounding line implementations. We have weakened the statements about the importance of model initialisation and instead emphasise the importance of perturbation history. Furthermore, we have addressed the notation inconsistencies and other minor points raised.

My main point regards the logical link that is made between the hysteretic response of the ice rise to sea level rise and the requirement for careful model initialisation (e.g. l.18 or l338-339). I am not completely sure that this association really holds. Don't get me wrong, I totally agree that careful initialisation of models is of prime importance when running transient simulations of the future evolution of ice sheets/shelves. I also agree that "the dynamics and buttressing effect of ice rises and ice rumples are dependent on the initial geometry prescribed, which is typically unknown" (l.319-320). I see clearly the link between the hysteretic behavior and some form of irreversibility: if the system is forced with a given perturbation from a given initial steady state, it does not come back to the same steady state when the perturbation is removed. However, it does not necessarily mean it will behave dramatically differently if you start from a slightly different initial state, as long as the perturbation pattern is similar (i.e. in your case, sea level increase or sea level decrease). A good illustration of this point is the second cycle of perturbation that you impose for the low friction scenario: the initial steady state from which the system starts for this second cycle is different from the one of the first cycle, and yet the dynamical evolution of the grounded area and buttressing effect become relatively rapidly similar to that of the first cycle (dotted lines are 'rapidly' superimposed to solid lines in Figs. 8a-c). Once again, I have the feeling that it is more the history of the perturbation (are we in a sea level increase or decrease phase ?) that is of importance rather than the initial state.

Response: Agreed, and thank you for raising this point. We have changed the sentence "This hysteresis not only shows irreversibility following an equal increase and subsequent decrease in sea level, but also has important implications for ice flow model initialisation." (originally line 18) to "This hysteresis not only shows irreversibility following an equal increase and subsequent decrease in sea level, but also shows that the perturbation history is important when the ice rise or ice rumple geometry is not known.". Furthermore, we have changed the sentence "As a consequence of this behaviour, we identify the need for careful consideration of the grounded area of an ice rise during model initialisation in order for the correct feature to form." to "As a consequence of this behaviour, we identify the importance of perturbation history for the formation of the correct feature." (originally lines 338-339).

Another point regards the presentation of the SIA model (Sect. 2.3 and 2.4). It seems to me that it is largely inspired from Greve and Blatter (2009), and some notations become inconsistent with the ones that were used to introduce the full-Stokes model in Sect 2.1. See specifics comments. Finally, there are a few points that, in my opinion, lack of clarity. First, I would write straight away in the abstract that you are running synthetic experiments and not dealing with real-world applications. Second, the fact that the comparison between the full-Stokes and SIA surface velocities is done for the initial steady states only would benefit to be stated more clearly in the text.

Response: Agreed. The notation inconsistencies have been rectified (see replies below). We have added to the abstract that we are studying idealised ice rises and ice rumples in the form of the sentence, "We investigate this behaviour using a three-dimensional full Stokes ice flow model with idealised ice rises and ice rumples.". We have changed the title of Section 3.1 from "Steady state analysis" to "Steady state analysis before sea level perturbation" so that it is clear that the SIA comparison is only done for the initial steady states.

Finally, although it is never clearly mentioned in the text (unless I missed something), it seems from Figs.3-8-9-10 that the sea level decrease experiments are continued after the initial 0 m level has been recovered. If this is true, this would deserve some explanation in the text.

> **Response: Agreed. This was not explained well. We have now added the sentence "Furthermore, we run branches of the simulation beyond the original sea level at the same sea level decrease rate of 0.02 m a^{-1}." to Section 2.5**

Below, I list some specific comments.

Specific comments

RV1.1: P2 L30: 'control' ! Is that not too strong ? What about 'influence' or 'affect' ?

> **Response: "control' changed to "influence'**

RV1.2: P2 L46-47: 'simpler ice-flow approximations' ! shouldn't it be singular ?

> **Response: This indeed was not strictly correct. We have changed this part of the sentence to "we compare the full Stokes solutions with the shallow ice approximation (Hutter, 1983; Greve and Blatter, 2009) and the Vialov profile (Vialov, 1958)),"**

RV1.3: P4 L62: I think there should be a minus sign in front of g as the vertical unit vector is pointing upward.

> **Response: Agreed. The minus sign was originally included in the table. We have now taken it out of the table and added it to the following equation:**
>
> $\mathbf{g} = -g\hat{\mathbf{e}}_z$

RV1.4: P4 L64: The 0 should not be bold as the divergence of a vector is a scalar.

> **Response: Fixed.**

RV1.5: P4 L76: Here, the vector u represents the velocities at the surface/base, which should be precised. There is an additional constraint that you did not mention and that is of importance for the grounded part, i.e. $b(x, y) \leq zb(x, y, t) \leq zs(x, y, t)$ where b represents the bed elevation.

> **Response: Agreed. We have added this condition to the text.**

RV1.6: P5 L82: How do you tune this 'tuning parameter' ?

> **Response: The value was deemed appropriate during initial model setup based on the fact that this particular parameter choice gave reasonable basal melt rates that allowed the formation of an ice rise.**

RV1.7: P5 L82: 'the closest' ! what do you mean by 'the closest' ?

> **Response: By "closest", we wanted to specify that it is not just any point on the grounding line (GL) that is used in the calculation of the distance from the grounding line, but only the GL node closest to the current node during computation. We have removed the word "closest" and added the following sentence for clarification: "During computation, x represents the position of the current node and $\mathbf{x_g}$ represents the position of the grounding line node closest to the current node."**

RV1.8: P5 L85: 'no friction' ! I find more natural to speak about 'free-slip', but it is a matter of choice.

> **Response: Agreed, "no friction" changed to "a free-slip condition"**

RV1.9: P5 L91: Why did you choose the 'First Floating' implementation ? You are dealing with Weertman friction law with constant friction coefficients, which induces a discontinuity of friction at the GL on the mathematical level. The proper way to represent this discontinuity in the FEM numerical framework of Elmer is to use the 'Discontinuous' implementation. Using the 'First Floating' implementation, you artificially impose a linear decrease of friction over all the last grounded elements due to the interpolation of friction parameters at the integration points from their nodal values through the FEM basis functions. This choice could be justified by the fact that, on the physical level, one would expect a smooth transition of friction from its value on the grounded part to zero at the GL. If that was your reasoning when choosing the FF implementation, then it would be worth to state it clearly in the text.

RV1.10: P6 L103: According to Gagliardini and others (2016), with such a resolution of 350 m, the GL behavior keeps being sensitive to the numerical treatment of friction at the GL (i.e. First Floating, Last Grounded or Discontinuous implementations). This is an additional reason to give a clear justification for your choice of the FF implementation.

> **Response: Thank you for raising this point. We have run an equivalent simulation using the *Discontinuous* grounding line implementation and have added a comparison plot in the appendix (Fig. B1 in Appendix, also shown here as Fig. 1) showing the response of the grounded area to sea level perturbation. Furthermore, we have added the following text in the appendix: "In the case of the *low* basal friction scenario, we have run equivalent simulations using a differing grounding line numerical implementation, namely the *Discontinuous* method (Fig. B1). At the grounding line, basal friction is applied if the other two nodes in the element are also grounded and a free-slip condition is applied if the other two nodes are ungrounded. The *First Floating* numerical implementation, however, assumes a free-slip condition at the grounding line and a linear reduction in basal friction between it and the upstream node is applied. Although the *Discontinuous* numerical implementation has been shown to have the least dependence on mesh resolution, it can be argued that the *First Floating* is more plausible physically, with effective pressure disappearing at the grounding line (Gagliardini et al., 2016). The simulations show that regardless of the numerical**

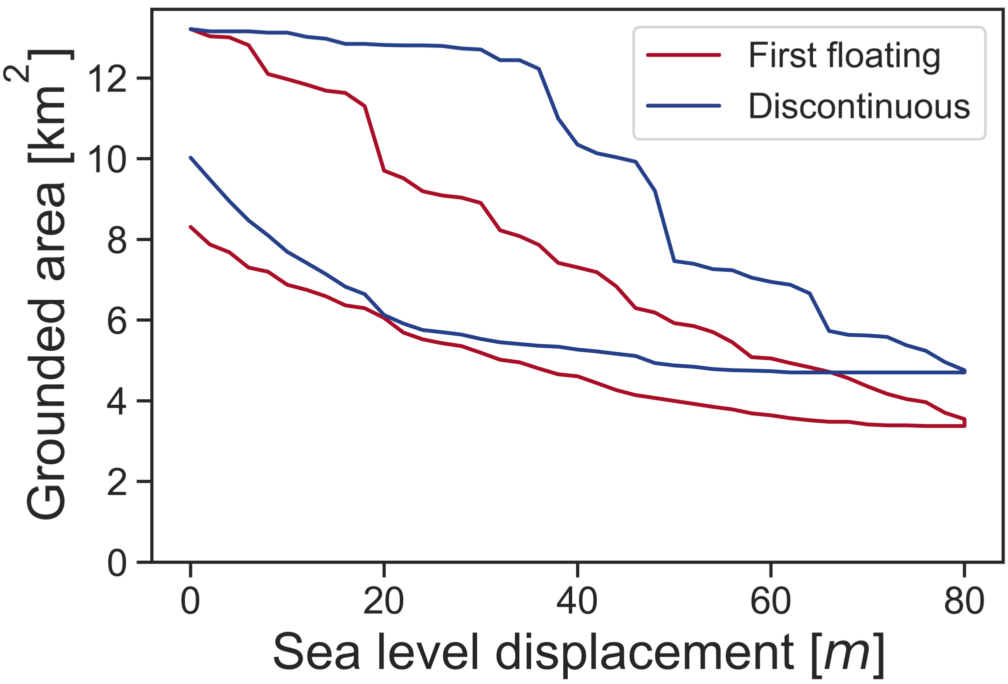

Figure 1: Shown is the response of the grounded area in the low friction case of the *First Floating* (red) and *Discontinuous* (blue) Elmer/Ice numerical grounding line implementations.

implementation, hysteresis occurs."

RV1.11: P6 L105: It would be worth precising the order of magnitude of considered time scales here, even if it becomes clearer later in the text.

Response: Agreed, "time scales" changed to "glacial-interglacial time scales".

RV1.12: P6 Eq10: It is strange that you switch from zs to h and from zb to b to denote the surface/base elevations. It feels like you have taken Eq. (5.84) of Greve and Blatter (2009) without adapting the notation to your own work.

Response: Agreed. We have changed h to z_s and H to $(z_s - z_b)$. We have left b as is because it refers to the bed, whereas z_b refers to the bottom ice surface (i.e. the ice surface in contact with the ocean or bed).

RV1.13: P6 Eq11: Same remark as above, plus I don't understand the purpose of the subscript h for the gradient operator. First, it does not appear in Eq. (10). Second, h being the surface elevation (your zs), it does obviously not depend on z so that the gradient operator does only consist in the x and y components. In addition, in the first occurence of the gradient operator in Eq. (11), the subscript is not at the proper position.

Response: Agreed, we have removed the subscripts and removed the sentence, "Here, ∇_h denotes the two-dimensional, horizontal gradient operator."

RV1.14: P6 Eq12: Here again, the formulation of Greve and Blatter (2009) would require some adaptations to your own case. More precisely, this expression is not directly consistent with the way the basal shear stress is defined in Eq. (8). In Greve and Blatter (2009), the effect of the normal stress Nb on the basal shear stress is explicited in the formulation of the friction law (5.35), while most of the time this effect is hidden in the friction parameter C of the Weertman law. I know that Eq. (13) is intended to establish the consistency between the two formulations, but in that case I think there should be a minus sign in Eq. (13) (or in Eq. (8), but you have to choose), and the exponents p and q that appear in Eq. (12) would need to be defined somewhere. In your case q = 1 and p = 1=m. I think it would be cleaner to have Eq. (12) formulated directly consistently with Eq. (8).

Response: We agree that there is an inconsistency in the minus signs which stems from the choice of representation of stress as either the driving force or basal drag in the stress-velocity relationship. We have changed Eq. 8 to

$$\boldsymbol{\tau}_b = -C|\mathbf{u}_b|^{m-1}\boldsymbol{u}_b, \tag{1}$$

to include a minus sign. We have also added the sentence "In Eq. (12), p and q are chosen for consistency with the non-linear Weertman-type friction law described above.", and the values are provided in the parameter table. We have not reformulated either equation as we wanted to use the common representation of each equation.

RV1.15: P6 Eq13: See comment above.

Response: See reply directly to *RV1.14*

RV1.16: P6 Eq17: Here, the expression of h0 does not correspond to the one in Eq. (5.117) of Greve and Blatter (2009). Could you double-check ?

Response: Yes, the expression of h_0 differs by a factor of 2 in the denominator below $\dot{a}_s$. The reason is the use of a radial/polar flux condition compared with the standard Cartesian coordinate formulation. When Eq. (5.107) in Greve & Blatter (2009) is expressed in polar coordinates, whilst assuming no azimuthal variance, Eq. (15) is obtained. Integrating, we obtain $Q_R(R) = \dot{a}_s R/2$ in contrast to $Q(x) = \dot{a}_s x$ (Eq. (5.115) in Greve & Blatter (2009)). Further calculations, analogous to page 86 in Greve & Blatter (2009), result in the extra factor of 2 in the denominator in the expression of h_0.

RV1.17: P8 Fig. 3: The Fig. is not consistent with the main text of Sect. 2.5: the decrease of sea level seems to continue further below the initial 0 m level (green and red lines), while the text says that "Sea level is then decreased at a rate of 0.02 m a^{-1} back to the initial level followed by a second phase of constant sea level for 2000 years."

Response: Agreed. This was not explained well. We have now added the sentence

"Furthermore, we run branches of the simulation beyond the original sea level at the same sea level decrease rate of 0.02 m a^{-1}." to Section 2.5

RV1.18: P8 L148: "with ice being frozen to the bed" ! "mimicking ice frozen to the ground" ?

Response: Agreed. Changed to "mimicking ice frozen to the bed."

RV1.19: P9 L162: "characteristic timescale" ! I have a hard time to figure out what does this quantity represents physically. Maybe, it requires more explanation or maybe you can simply drop it as it is not used anywhere else later on.

Response: Agreed. We have added the sentence "The characteristic timescale is a metric that gives an indication of the rate of development of Raymond arches (Martín et al., 2009; Goel et al., 2020).".

RV1.20: P9 L189-190: "the upstream ice shelf velocities" ! it is not very clear what velocities exactly you are referring to, and how you can get a single value of velocity. You give a brief explanation in the caption of Fig. 9, but some precisions would be required here too.

Response: Agreed. We have added the sentence "The upstream ice shelf velocity is defined as the mean velocity of ice in the x-direction at $x = 20$ km, as marked by Label (1) in Fig. 1c."

RV1.21: P10 Fig. 4: You should precise that the velocities are the full-Stokes ones (are they ?).

Response: Agreed. We have now specified in the caption that the velocities are the full Stokes velocities.

RV1.22: P11 Fig. 5: What is represented exactly ? Is is $|v_{Stokes} - v_{SIA}|/|v_{Stokes}|$? If yes, wouldn't it be more interesting to represent $(|v_{Stokes}| - |v_{SIA}|)/|v_{Stokes}|$, so that we could tell when the full-Stokes surface velocities are higher than the SIA ones and conversely ?

Response: Agreed. We have now plotted $100 \times (|v_{Stokes}| - |v_{SIA}|)/|v_{Stokes}|$ rather than $100 \times |v_{Stokes} - v_{SIA}|/|v_{Stokes}|$.

RV1.23: P12 L215: "at sea-level displacements of" ! this term is confusing as we are in the sea-level decrease phase. What about something like "when sea level is back to 21 and 19m above initial level".

Response: Agreed. We have replaced the text with the sentence "... when sea level is 21 and 19 m above the initial sea level in the..."

RV1.24: P13 L223: "and independent of the initial conditions" ! I am not sure that this formulation is appropriate as you have actually shown that, depending on the initial state, the system might or might not go back to its initial state. I would rather say something like "The hysteresis cycles are now closed with the final steady state corresponding to the initial one".

Response: Agreed. We have changed the sentence to "The hysteresis cycle is now closed, with the final steady state corresponding to the state before the last sea level perturbation cycle."

RV1.25: P13 L226: It is not completely clear that the state obtained after the sea level is back to the initial 0 m level is a "viable state" (you mean a steady state, right ?), as it seems that you are keeping decreasing sea level below this initial reference.

Response: Only the initial state is in steady state and the second state at 0 m is indeed a transient state. We have changed the word "viable" to "differing" so it is not interpreted as meaning "steady state".

RV1.26: P14 Fig.8: "The crosses represent the results of steady state branches of the transient simulations at corresponding sea levels." ! This is not very clear to me. How can you be sure that these are steady states while you keep increasing/decreasing sea-level ?

Response: What we have done is run branches of the simulation to steady state at the specified sea levels, keeping sea level fixed. For clarity, we have added the sentence "Branches of the *low* basal friction simulation are run to steady state at discrete intervals while keeping sea level fixed. We run these simulation branches in order to understand how far from steady state the transient simulations are. This gives an indication of how transient simulations with lower absolute increase and decrease rates would evolve." to Section 2.5.

RV1.27: P14 L253-254: "the ad hoc grounding line positions of the full Stokes model" ! I don't quite like this expression as it sounds a bit like if this GL position was fixed arbitrarily, while it is actually the most rigorous way to define it. Indeed, in the hydrostatic approximation there is the assumption that the stress in a horizontal plane is purely vertical and equals the weight of the overlying ice column (i.e. shear stresses txz and tyz are neglected), which allows to deduce the GL position from the flotation criterion. In contrast, in full-stokes such assumption is not made, and a contact problem must be solved in which the normal stress at the ocean/ice interface (which is not necessarily purely hydrostatic this time) is compared to the sea water pressure.

Response: Agreed. We have removed the words "ad hoc".

RV1.28: P16 Fig. 11: 'blue lines' ! Do you mean 'solid lines' ?

Response: Yes, we have changed "blue lines" to "solid lines".

RV1.29: P16 Fig. 11: 'after an equal increase and decrease in sea level.' ! 'after a full cycle of sea level increase and decrease'?

Response: Agreed. We have changed the text to read "... after a full cycle of sea level increase and decrease.".

RV1.30: P17 Fig. 17: Panel (b) is the intermediate friction scenario and not the high friction scenario, right ?

Response: Agreed. Text changed from "high" to "intermediate".

RV1.31: P18 L280-282: I have a hard time to understand your point. Could you explain ?

Here we explain the counterintuitive result that surface velocities on the ice rumple are lower in the *low* friction scenario compared to *intermediate* friction scenario. The reason is that in the *low* friction scenario the total grounded area is larger compared to the *intermediate* friction scenario. It might be worth investigating whether inverse techniques used to predict the basal friction coefficient beneath pinning points reproduce these results, e.g., regardless of horizontal resolution applied. We have changed the text: 'Interestingly, the *low* friction ice rumple exhibits lower minimum velocities than the *intermediate* friction ice rumple most, likely due to a greater grounded area (Fig. 12). It is worth investigating whether inverse techniques used to predict the basal friction coefficient beneath pinning points produce results which remain valid regardless of horizontal resolution applied.' "

RV1.32: P18 L303-304: I don't understand this point. Could you reformulate to make it clearer ?

Response: Agreed, the previous formulation resulted in possible misinterpretation. We have re-worded the paragraph as, "A self-stabilising feedback occurs, with divide migration opposing grounding line retreat in a sea level increase scenario. The ice rise height reduces and the divide migrates stossward during lee side grounding line retreat. Because the divide moves stossward, the area of accumulation adjacent to the divide on the lee side of the ice rise increases. The increased accumulation area promotes an increased flux across the grounding line, opposing grounding line retreat. Analogously, sea level decrease results in leeward divide migration. The resulting reduction in accumulation area adjacent to the divide on the lee side of the ice rise opposes grounding line advance. The existence of negative feedback mechanisms in both the sea level increase and decrease scenario result in hysteretic behaviour (Figs. 8, 9 and A1)."

RV1.33: P19 L330: 'full Stokes velocities with SIA velocities' ! 'full Stokes steady velocities with SIA steady velocities' ?

Response: Agreed. We have changed the sentence to read "..simulated steady state full Stokes velocities with steady state SIA velocities...".

RV1.34: P19 L331: 'due to a greater influence of stresses from the surrounding ice shelf' ! 'due to stronger mechanical coupling to the surrounding ice shelf' ?

Response: Agreed. Text changed to "due to stronger mechanical coupling to surrounding ice shelf".

2 Reply to Anonymous Referee #2

This paper presents modelling experiments designed to test the responses of ice rises and rumples to perturbations in sea level under different basal friction conditions. It demonstrates hysteretic behaviour in velocities and profiles of ice rises, with two distinct possible steady states. Repeated tests in one case show that one of these steady states is stable, with further perturbations to sea level responding in a closed hysteretic loop. Additionally, comparisons are made between results using full Stokes model and an SIA approximation, showing minimal difference with a high friction case, but a large mismatch when greater basal sliding is allowed. I found the majority of the manuscript to be well written and easy to follow. However, in some places the paper in its current form lacks clarity and precision. Some more attention needs to be given to the presentation of the equations in the early sections, where there are cases of conflicting notation and variables which are not defined. Part of the experimental setup described in the text is contradicted by some of the figures, namely whether the sea level is reduced back to its original state, or in fact lowered beyond the initial value. Another aspect I was unclear on is the presentation of "equilibrium states" on some figures, which did not appear to be addressed in the text (perhaps I somehow missed it, in which case it should be made clearer). Specific comments are listed below. Overall, I found this to be an interesting study, with novel and useful results. The methodology is rigorous, and the manuscript is well structured. It is certainly worthy of publication in the Cryosphere subject to revisions which address the issues of clarity.

> **We would like to thank the referee for their encouraging review of our manuscript. We have addressed the issue of missing information in the model setup section describing the lowering of sea level below the original sea level in Section 2.5. We have indicated in the manuscript that we use the terms "steady state" and "equilibrium state" interchangeably and have added text to clarify how the steady states are reached (see RV1.14 below). Furthermore, we have addressed issues raised regarding the presentation of the equations and other minor points.**

Specific comments

RV2.1: Line 21 – I think you start off with "Great progress in ice flow modelling" or similar, just to make it entirely clear right at the start.

> **Response: Agreed. We have changed the sentence accordingly.**

RV2.2: Line 49 – Maybe you should briefly explain what a Vialov profile is. Just a short phrase such as "the solution to an idealised analytical problem".

> **Response: Agreed. We have now added the following to the sentence: "...between the full Stokes ice thickness and the Vialov profile, an idealised solution for the ice geometry.**

RV2.3: Figure 1 – In panel (c) I would suggest labelling the cross sections as 1-3 and labelling the dome using a letter to differentiate it. I was also confused a little upon first glace by the arrow pointing to the ice dome being the same line type as the cross sections.

Response: We have altered the figure, marking the cross-sections as 1-3 and the dome with the letter "D"

RV2.4: Line 61 – Should the gravity term be negative, since your z-axis point upwards?

Response: Agreed. The minus sign was originally included in the table. We have now taken it out of the table and added it to the following equation:

$\mathbf{g} = -g\hat{\mathbf{e}}_z$

RV2.5: Line 73 – I'd put the trace operation in non-italic font, to distinguish from variables.

Response: Agreed. We have now used non-italic font for the trace operator.

RV2.6: Line 76 – You should probably use us,b to be entirely clear.

Response: We have not made any changes here, as it is already apparent that the condition applies only to the upper and lower surface nodes and that at a numerical level, only the velocities at those nodes are used to make the calculations. The same applies, for example, to the boundary condition $\mathbf{u} \cdot \mathbf{n} = 0$, where we do not specify within the equation that we mean the boundary velocities.

RV2.7: Line 96 – M needs to be defined in the text.

Response: Agreed. We have added "M is the amplitude of the bed anomaly"

RV2.8: Line 104 – This should be added to the reference list and cited as usual.

Response: Agreed. Cited in text and added to reference list.

RV2.9: Line 115 – You've introduced h here when you already have zs defined. If this is a different quantity (eg. the reference plane isn't the same as z=0) this should be made clear. If not, you should be consistent with notation.

Response: Agreed. We have replaced h with z_s and H with $(z_s - z_b)$. See also reply to *RV1.12*.

RV2.10: Line 118 – The standard and subscript h are the wrong way round in the first instance on this line.

Response: Agreed. We have removed the subscripts completely as suggested by reviewer one.

RV2.11: Line 120 – This equation is quite confusing within the context of this paper. It's written in quite a convoluted way, and it would be far clearer if it were formulated in the same way as equation 8, especially as it is directly related by the following equation. Also, p and q are not defined.

Response: We have decided to keep the differing formulations for the FS and SIA basal friction parameterisations as the respective formulations are commonly written in these forms in the literature for Elmer/Ice and SIA. We have added the sentence, "In Eq. (12), p and q are chosen for consistency with the non-linear Weertman-type friction law described above."

RV2.12: Line 130 – The variables Q, R and QR in this equation need to be defined in the text.

Response: Agreed. We have added definitions to the text.

RV2.13: Line 132 – Same as above for L.

Response: Agreed. We have added "L is the horizontal distance from the ice rise divide to the grounding line"

RV2.14: Figure 3 – I'm not clear about what the "equilibrium simulations" are. These don't seem to be referred to in section 2.5. More explanation is needed so that this can be understood. They are also referred to as "steady state branches". Does this mean that new experiments branch off from these points in which the sea level is kept the same until a steady state is reached?

Response: Yes, by equilibrium simulation, we mean steady state simulation. We have added the term to Section 2.5 in the sentence, "Branches of the *low* basal friction simulation are run to steady state (equilibrium) at discrete intervals while keeping sea level fixed."

RV2.15: Line 150 – The green line in Figure 3 shows this 0.02ma^{-1} decrease continuing until it reaches -40m, rather than the last 2000 years being flat. I assume this is an error in the plot?

Response: This is not an error in the plot. We had not explained this previously, but we have now added the sentence "Furthermore, we run branches of the simulation beyond the original sea level at the same sea level decrease rate of 0.02 m a^{-1}." to Section 2.5.

RV2.16: Line 152 – Why was a second cycle only done for one friction case?

Response: A second cycle was performed only on one friction case because of computation time. One sea level perturbation cycle took roughly 4 weeks to simulate.

RV2.17: Line 159 – This should probably be specified as being analysis of the initial steady states for clarity, since there are also different final steady states and the branches referenced in the caption of Fig. 3.

Response: Agreed. We have changed the name of section 3.1 from "Steady state analysis" to "Steady state analysis before sea level perturbation"

RV2.18: Line 160 – Is this referring to full Stokes or SIA? I assume full Stokes, but you should be clear.

> **Response: we have added "full Stokes" to the sentence.**

RV2.19: Line 189 – "and" rather than "as well as".

> **Response: Agreed and changed.**

RV2.20: Figure 5 – I assume these are the initial steady states? This should be stated in the caption, perhaps specifying the time (t=2000, if I'm correctly interpreting this?).

> **Response: Agreed. We have added time to the caption and have also stated that the figures correspond to steady states.**

RV2.21: Figures 6 & 7 – Again, specify in the captions what time these velocities and cross sections are for.

> **Response: Agreed. Time added to captions.**

RV2.22: Line 222-3 – I think what you're saying here is that from the final steady state obtained after one full perturbation cycle, further perturbations in sea level do not cause changes to the steady state position? Figure 8 is very clear in this regard, but I think there's probably a better way of wording it. Do you know if the same would be true of the intermediate and high friction cases?

> **Response: Agreed and rephrased from "The hysteresis cycles are now closed and independent of the initial conditions." to "The hysteresis cycle is now closed, with the final steady state corresponding to the state before the last sea level perturbation cycle."**

RV2.23: Figure 8 – Are panels (b) and (d) really needed? I suppose the transition points are in slightly different places? It's still unclear to me what the "equilibrium states" are, as noted for Fig. 3 above.

> **Response: We decided to keep the panels (b) and (d) as the dashed line is covered by the solid lines in (a) and (c) in a large part of the plot.**

RV2.24: Figure 10 – I notice the sea level goes below 0 at the end again here. I assumed it was a mistake in Fig. 3, as I don't think this decrease in sea level was mentioned in the text. Was it actually part of the experiment and if so why has it not been mentioned?

> **Response: We have added the sentence "Furthermore, we run branches of the simulation beyond the original sea level at the same sea level decrease rate of** 0.02 **m a-1." in Section 2.5**

RV2.25: Figure 11 – I think you mean "solid" rather than "blue".

Response: Agreed and changed.

RV2.26: Figure 12 - Specifying the time would be nice here.

Response: Agreed. Time added to caption.

RV2.27: Appendix A – It seems a little odd to have a single figure with no text as an appendix. Can this figure not just be included within the main text, or is there some appendix text missing?

Response: Thank you for raising this point. We have added text describing the figure and comparing it with the *low* basal friction scenario.

References

O. Gagliardini, J. Brondex, F. Gillet-Chaulet, L. Tavard, V. Peyaud, and G. Durand. Brief communication: Impact of mesh resolution for MISMIP and MISMIP3d experiments using Elmer/Ice. *The Cryosphere*, 10(1):307–312, Feb. 2016. doi: 10.5194/tc-10-307-2016.

V. Goel, K. Matsuoka, C. D. Berger, I. Lee, J. Dall, and R. Forsberg. Characteristics of ice rises and ice rumples in Dronning Maud Land and Enderby Land, Antarctica. *Journal of Glaciology*, 66(260):1064–1078, Dec. 2020. doi: 10.1017/jog.2020.77.

R. Greve and H. Blatter. *Dynamics of ice sheets and glaciers*. Springer, Dordrecht, 2009.

K. Hutter. *Theoretical glaciology: material science of ice and the mechanics of glaciers and ice sheets*. Dordrecht, D. Reidel Publishing Co./Tokyo, Terra Scientific Publishing Co., 1983.

C. Martín, R. C. A. Hindmarsh, and F. J. Navarro. On the effects of divide migration, along-ridge flow, and basal sliding on isochrones near an ice divide. *Journal of Geophysical Research*, 114(F2): F02006, Apr. 2009. doi: 10.1029/2008JF001025.

S. Vialov. Regularities of glacial shields movement and the theory of plastic viscous flow. *Physics of the Movements of Ice IAHS*, 47:266–275, 1958.

Hysteretic evolution of ice rises and ice rumples in response to variations in sea level

A. Clara J. Henry[1,2,3], Reinhard Drews[2], Clemens Schannwell[1], and Vjeran Višnjević[2]

[1]Max Planck Institute for Meteorology, Bundesstr. 53, 20146 Hamburg, Germany

[2]Department of Geosciences, University of Tübingen, Schnarrenbergstr. 94-96, 72076 Tübingen, Germany

[3]International Max Planck Research School on Earth System Modelling, Max Planck Institute for Meteorology, Hamburg, Germany

Correspondence: Clara Henry (clara.henry@mpimet.mpg.de)

Abstract. Ice rises and ice rumples are locally grounded features found in coastal Antarctica and are surrounded by otherwise freely floating ice shelves. An ice rise has an independent flow regime, whereas the flow regime of an ice rumple conforms to that of the ice shelf and merely slows the flow of ice. In both cases, local highs in the bathymetry are in contact with the ice shelf from below, thereby regulating the large-scale ice flow, with implications for the upstream continental grounding line position. This buttressing effect, paired with the suitability of ice rises as a climate archive, necessitates a better understanding of the transition between ice rise and ice rumple, their evolution in response to a change in sea level, and their dynamic interaction with the surrounding ice shelf. We investigate this behaviour using a three-dimensional full Stokes ice flow model with idealised ice rises and ice rumples. The simulations span end-member basal friction scenarios of almost stagnant and fully sliding ice at the ice-bed interface. We analyse the coupling with the surrounding ice shelf by comparing the deviations between the non-local full Stokes surface velocities and the local shallow ice approximation (SIA). Deviations are generally high at the ice divides and small on the lee sides. On the stoss side, where ice rise and ice shelf have opposing flow directions, deviations can be significant. Differences are negligible in the absence of basal sliding where the corresponding steady state ice rise is larger and develops a fully independent flow regime that is well described by SIA. When sea level is increased and a transition from ice rise to ice rumple is approached, the divide migration is more abrupt the higher the basal friction. In each scenario, the transition occurs after the stoss side grounding line has moved over the bed high and is positioned on a retrograde slope. We identify a hysteretic response of ice rises and ice rumples to changes in sea level, with grounded area being larger in a sea level increase scenario than in a sea level decrease scenario. This hysteresis not only shows irreversibility following an equal increase and subsequent decrease in sea level, but also ~~has important implications for ice flow model initialisation~~shows that the perturbation history is important when the ice rise or ice rumple geometry is not known. The initial grounded area needs to be carefully considered, as this will determine the formation of either an ice rise or an ice rumple, thereby causing different buttressing effects.

1 Introduction

Great progress in ice flow modelling has improved the physical representation of dynamical processes at the margins of the Antarctic ice sheet, but the transient evolution of the grounding line continues to be challenging, requiring high mesh resolution, small time steps and advanced model physics (Schoof, 2007; Goldberg et al., 2009; Gudmundsson et al., 2012; Haseloff and Sergienko, 2018; Sergienko and Wingham, 2022). Moreover, the lack of past observational constraints and ice sheet model initialisation inconsistencies result in spin-up simulation geometries which differ from observations (Seroussi et al., 2019) and result in parameter choice uncertainty (Albrecht et al., 2020).

Ice rises and ice rumples are locally grounded features surrounded by floating ice shelves and play a dual role in this context. Firstly, ice rises and ice rumples regulate the flow of ice towards the ocean through their buttressing effect (Favier and Pattyn, 2015; Barletta et al., 2018; Reese et al., 2018; Still et al., 2019; Still and Hulbe, 2021; Schannwell et al., 2020) and ~~control~~ influence the migration of the continental grounding line (Favier et al., 2012). Secondly, past adjustments in local ice shelf flow dynamics can be inferred from ice rises by investigating, for example, isochronal structure and the development of features such as Raymond arches within ice rises (Raymond, 1983; Martín et al., 2006; Gillet-Chaulet and Hindmarsh, 2011; Hindmarsh et al., 2011; Drews et al., 2013, 2015; Schannwell et al., 2019; Goel et al., 2020). The importance of ice rise formation and decay for continental ice sheet evolution (e.g., due to glacial isostatic uplift or changes in sea level) have been recognised in a number of scenarios and show the key role that ice rises play in large-scale grounding line migration patterns over glacial cycle timescales (Bindschadler et al., 1990, 2005; Barletta et al., 2018; Kingslake et al., 2018; Wearing and Kingslake, 2019).

In adopting terminology from Matsuoka et al. (2015), we identify ice rises as prominent grounded features with a distinct local radial flow regime, causing the flow of the surrounding ice shelves to divert either side of the feature. Ice rumples, however, generally form on less prominent bed highs and result in a predominantly unidirectional flow regime with the upstream ice shelf flowing over the bed anomaly. Ice rises and ice rumples are found all around the perimeter of the Antarctic Ice Sheet, but the mechanisms governing the transition from one flow regime to the other have not yet been investigated and influences of the surrounding ice shelves on the local flow regimes have not yet been quantified. In order to explore these questions, we use the three-dimensional, full Stokes model Elmer/Ice to simulate idealised ice rises and ice rumples under various basal friction scenarios and sea level perturbations.

To quantify non-local effects from the surrounding ice shelves, we compare the full Stokes solutions with ~~simpler ice-flow approximations (e.g.,~~ the shallow ice approximation ~~Hutter (1983); Greve and Blatter (2009))~~(Hutter, 1983; Greve and Blatter, 2009) and the Vialov profile (Vialov, 1958)), which do not capture the stress transfer between ice shelf and ice rise. Furthermore, we investigate whether the locality of flow and basal sliding can be determined by examining the mismatch between the ~~Vialov profile and the observed ice thickness~~full Stokes ice thickness and the Vialov profile, an idealised solution for the ice geometry. Using sea level perturbations, we explore whether ice rises and ice rumples respond hysteretically and whether multiple steady states exist for a given set of boundary conditions by tracking the grounded area, upstream ice shelf velocity and dome position. Additionally, we investigate under which formation scenarios ice rumples reach a steady state and under which scenarios they are merely a transient feature during ice flow reorganisation.

2 Methods

Ice rises and ice rumples, and their surrounding ice shelves are investigated in steady state and transient scenarios using the three-dimensional full Stokes numerical model Elmer/Ice (Gagliardini et al., 2013).

2.1 Governing equations

We adopt a coordinate system in which the predominant along-flow direction is aligned with the x-axis, the predominant across-flow direction is aligned with the y-axis and the z-direction marks elevation relative to sea level. The flow of ice is governed by the full Stokes equations,

$$\boldsymbol{\nabla}\cdot\left(\boldsymbol{\tau}-\cancel{p}P\mathbf{I}\right)+\rho_i\mathbf{g}=0, \tag{1}$$

where $\boldsymbol{\tau}$ is the deviatoric stress tensor, ~~p~~ P is the pressure, ρ_i is the ice density and ~~$\mathbf{g}=g\hat{\mathbf{e}}_z$~~ $\mathbf{g}=-g\hat{\mathbf{e}}_z$ is the gravitational acceleration. We assume the ice to be incompressible, and so, the mass conservation equation reduces to

$$\boldsymbol{\nabla}\cdot\mathbf{u}=0. \tag{2}$$

The non-linear rheology of ice is modelled using Glen's flow law, which relates the deviatoric stress tensor, $\boldsymbol{\tau}$, to the strain rate tensor, $\dot{\boldsymbol{\epsilon}}$, as

$$\boldsymbol{\tau}=2\eta\dot{\boldsymbol{\epsilon}}, \tag{3}$$

where the effective viscosity, η, is

$$\eta=\frac{1}{2}A^{-1/n}\dot{\epsilon}_e^{(1-n)/n}. \tag{4}$$

Here, n is the Glen's flow law exponent, A is a rheological parameter primarily dependent on ice temperature. Since we assume ice to be isothermal, A is set to a constant value in all simulations. The effective strain rate, $\dot{\epsilon}_e$, is calculated from the strain rate tensor, $\dot{\boldsymbol{\epsilon}}$, as

$$\dot{\epsilon}_e=\cancel{\sqrt{tr(\dot{\boldsymbol{\epsilon}}^2)/2}}\sqrt{\mathrm{tr}(\dot{\boldsymbol{\epsilon}}^2)/2}. \tag{5}$$

2.1.1 Boundary conditions

The upper surface, $z=z_s(x,y,t)$, and lower surface, $z=z_b(x,y,t)$, evolve subject to

$$\left(\frac{\partial}{\partial t}+\mathbf{u}\cdot\boldsymbol{\nabla}\right)(z-z_{s,b})=\dot{a}_{s,b}, \tag{6}$$

where $\dot{a}_{s,b}$ are the accumulation / melt rates at the ice-shelf surface (s) and ice shelf base (b), respectively.

Furthermore, the grounded portion is constrained by the condition

$$b(x,y)\leq z_b(x,y,t)\leq z_s(x,y,t), \tag{7}$$

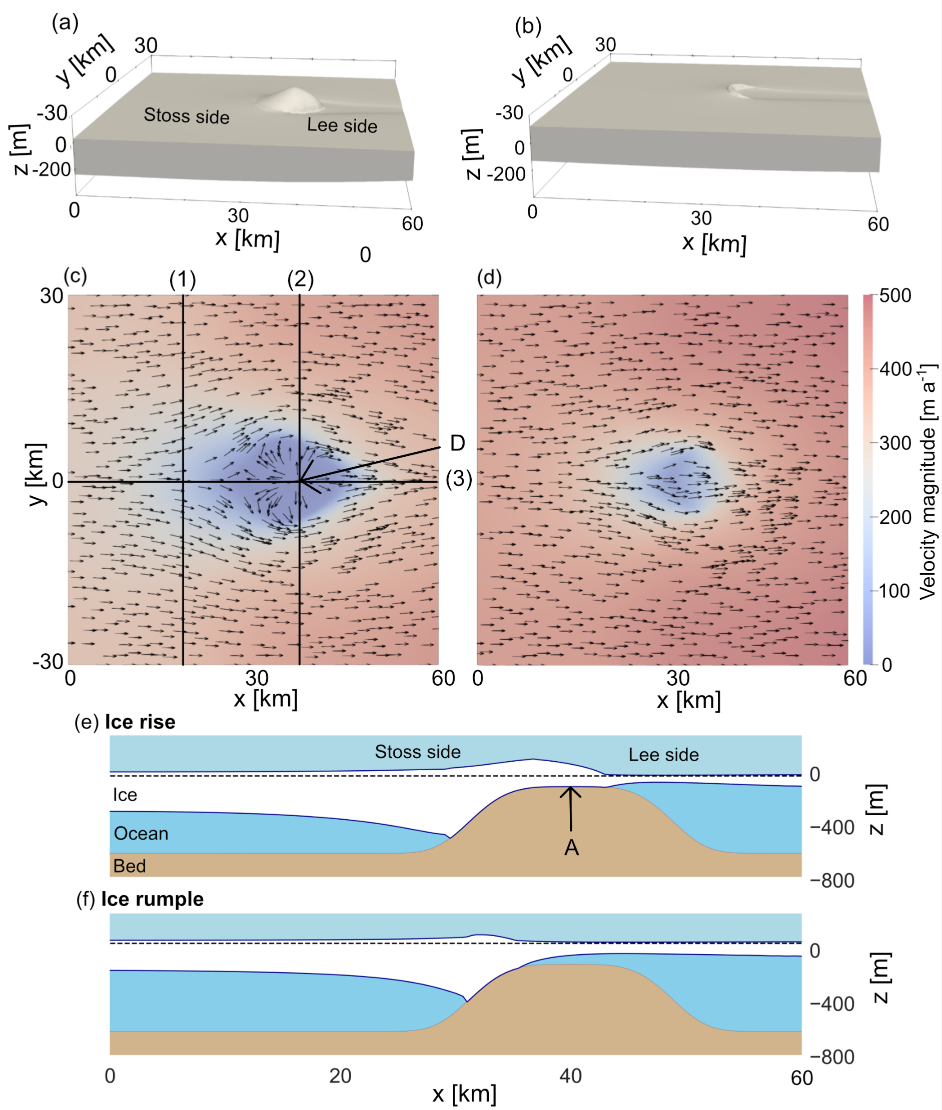

Figure 1. The 60×60 km model domain is shown in the case of (a) an ice rise and (b) an ice rumple. A corresponding bird's eye view in (c) and (d) show the surface velocity magnitude color coded and the ice flow direction with arrows. Corresponding along-flow cross-sections are shown in (e) and (f). Sea level is at an elevation of 0 m in the case of the ice rise and 80 m in the case of the ice rumple. In (c), (1), (2) and (43) indicate cross-sections used for analysis, and ~~(3)~~ D is the ice rise dome. Both (2) and (43) are cross-sections through the ice rise dome. In (e), A marks the highest point of the bed anomaly. The x-direction corresponds with the along-flow direction, the y-direction corresponds with the across-flow direction and the z-direction corresponds with the elevation.

where $b(x,y)$ is the bed. The surface accumulation rate, $\dot{a}_s = 1.2$ m a^{-1}, reflects the comparatively high rates observed at some ice rises in the Dronning Maud Land area of East Antarctica (Drews et al., 2013). The basal melt rate, $\dot{a}_b$, beneath the ice shelf

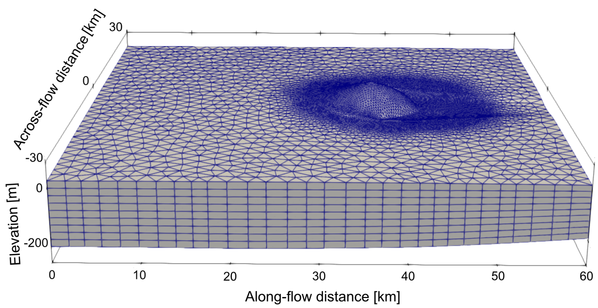

Figure 2. Shown is the mesh resolution of the mesh. In the horizontal, the mesh is unstructured and has a resolution of $350\ \mathrm{m}$ in the area surrounding the ice rise or ice rumple. The background resolution (of the surrounding ice shelf) is $2000\ \mathrm{m}$. The mesh is extruded in the vertical with 10 layers. Note that the geometry is exaggerated by a factor of 30 in the vertical direction.

is defined as a function of ice thickness, H, based on the parameterisation used in Favier et al. (2016),

$$\dot{a}_b = \begin{cases} 0, & \text{where ice is grounded, and} \\ \frac{1}{50} H^\alpha \tanh\left(\frac{|\mathbf{x}-\mathbf{x_g}|}{100}\right), & \text{where ice is floating,} \end{cases} \tag{8}$$

where α is a tuning parameter and $|\mathbf{x}-\mathbf{x_g}|$ is the ~~closest~~ distance to the grounding line. During computation, $\mathbf{x}$ represents the position of the current node and $\mathbf{x_g}$ represents the position of the grounding line node closest to the current node.

A constant flux of $Q\big|_{x=0} = 5.4 \times 10^9\ \mathrm{m^3 a^{-1}}$ into the domain is prescribed at the upstream boundary, corresponding to an initial velocity of $300\ \mathrm{ma^{-1}}$. Ice flows through a fixed calving front where ice is subject to sea pressure. At the lateral boundaries, ~~no friction~~ a free-slip condition is applied and the flow velocity is subject to the Dirichlet boundary condition $\mathbf{u} \cdot \mathbf{n} = 0$, where $\mathbf{n}$ is the normal vector pointing outwards.

Ice in contact with the bed is subject to a non-linear Weertman-type friction law,

$$\boldsymbol{\tau}_b = -C|\mathbf{u}_b|^{m-1}\boldsymbol{u}_b, \tag{9}$$

where $\boldsymbol{\tau}_b$ is the basal shear stress, C is a constant friction coefficient, $\boldsymbol{u}_b$ is the velocity tangential to the bed, and m is the friction law exponent. The position of the grounding line at each time step is determined by solving a contact problem (Durand et al., 2009). The continuous *First Floating* Elmer/Ice grounding line numerical implementation is used (Gagliardini et al., 2016) and was chosen because a discontinuity in basal friction at the grounding line caused undesired numerical artefacts in the ice surface.

2.2 Idealised model domain setup

The evolution of ice rises and ice rumples is simulated in a $60 \times 60\ \mathrm{km}$ domain (Fig. 1). A bed anomaly is introduced and allows isle-type ice rises and ice rumples to form. The bed takes the form $b(x,y) = b_0 + b_a$, where b_0 is a constant and b_a is an

Table 1. List of parameters used in the simulations

Parameter	Symbol	Value	Unit
Rheological parameter	A	4.6×10^{-25}	$\mathrm{Pa}^{-3}\,\mathrm{s}^{-1}$
Ice temperature	T	-15	C°
Glen's exponent	n	3	
Accumulation rate	$\dot{a}_s$	1.2	$\mathrm{m\,a}^{-1}$
Melt tuning parameter	α	0.76	
Glen's exponent	n	3	
Basal friction exponent	m	$1/3$	
Ocean density	ρ_w	1000	$\mathrm{kg\,m}^{-3}$
Ice density	ρ_i	900	$\mathrm{kg\,m}^{-3}$
Gravity	g	~~9.8~~ 9.8	$\mathrm{m\,s}^{-2}$
Bed base	b_0	-580	m
Maximum bed height (above b_0)	M	500	m
Bed anomaly extent parameter	σ	8	km
Bed anomaly centre	(x_0, y_0)	$(40, 0)$	km
SIA basal drag exponents	(p, q)	$(3, 1)$	

anomaly with a flat top, defined as

$$b_a(x,y) = M \exp\left\{ \frac{-((x-x_0)^2 + (y-y_0)^2)^2}{2\sigma^4} \right\}. \tag{10}$$

The centre of the bed anomaly is located at (x_0, y_0)~~and~~ , σ controls the horizontal extent and M is the amplitude of the bed anomaly. The shape of the bed anomaly is broadly consistent with observations of ice rises, many of which have a plateau-shaped top that is near horizontal (e.g., Derwael Ice Rise (Drews et al., 2015) and ice rises in the Fimbul Ice Shelf (Goel et al., 2020)). All parameters used in the model are summarised in Table 1.

The ice thickness is initialised to 300 m throughout the domain, resulting in a geometry that is predominantly floating with a small grounded area at the bed anomaly. To ensure adequate resolution at the grounding line and ice divide, the mesh is refined in the area encompassing the ice rise with a resolution of 350 m (Fig. 2). For this, we use the meshing software ~~Mmg (http://www. mmgtools.org/, version 5.3.10).~~ Mmg. This is in line with mesh resolution recommendations from other studies (Pattyn et al., 2013; Cornford et al., 2016), but is also the highest mesh resolution that is computationally feasible for the glacial-interglacial time scales considered here. To account for a possible migration of the ice rise, the radial extent of the area of high resolution is 5 km from the initial grounding line. In the remainder of the domain, a mesh resolution of 2000 m is used. The mesh is vertically extruded resulting in 10 layers spaced equally apart and the horizontal mesh size is kept constant throughout the simulations.

2.3 Shallow ice approximation (SIA) comparison

The shallow ice approximation (Hutter, 1983; Greve and Blatter, 2009) describes the flow of ice in the absence of longitudinal and transverse stress gradients and is composed of the deformational velocity ($\mathbf{u}_d$) and basal sliding velocity ($\mathbf{u}_b$) so that the total velocity is $\mathbf{u} = \mathbf{u}_d + \mathbf{u}_b$. In SIA, only the vertical shear stress gradients are considered, so that the x-direction and y-direction deformational components of the velocity take the form

$$\mathbf{u}_d = -2(\rho_i g)^n \boldsymbol{\nabla} \cancel{h} z_s |\boldsymbol{\nabla} \cancel{h} z_s|^{n-1} \int_b^z A(T')(\cancel{h} z_s - \bar{z})^n d\bar{z} \cancel{,}. \tag{11}$$

~~where $h(x,y)$ is the height of the ice surface relative to a reference horizontal plane. Here, $\boldsymbol{\nabla}_h$ denotes the two-dimensional, horizontal gradient operator.~~ We compare the velocity components only at the surface of the ice and also assume that temperature is constant, and so Eq. (11) reduces to

$$\mathbf{u}_d(x,y,\cancel{h} z_s) = -\frac{2A(\rho_i g)^n}{n+1} \cancel{H}(z_s - z_b)^{n+1} |\boldsymbol{\nabla} \cancel{h_h} z_s|^{n-1} \boldsymbol{\nabla}_{\cancel{h}} \cancel{h} z_s. \tag{12}$$

The x-direction and y-direction basal sliding components take the form

$$\mathbf{u}_b(x,y) = -C_b(\rho_i g \cancel{H}(z_s - z_b))^{p-q} |\boldsymbol{\nabla}_{\cancel{h}} \cancel{h} z_s|^{p-1} \boldsymbol{\nabla}_{\cancel{h}} \cancel{h} z_s. \tag{13}$$

where ~~H is the ice thickness and~~ C_b is the basal friction coefficient and relates to the full Stokes basal friction coefficient, C, as follows:

$$C_b = \frac{N_b}{C^{1/m}} \tag{14}$$

with

$$N_b = \rho_i g \cancel{H}(z_s - z_b), \tag{15}$$

where $\mathbf{N}_b = N_b \mathbf{e}_z$ is the basal normal stress. In Eq. 13, p and q are chosen for consistency with the non-linear Weertman-type friction law described above.

2.4 Comparison with the Vialov approximation

The Vialov profile (Vialov, 1958) is an analytical solution for an ice sheet profile in the case of a non-slip, flat bed and constant accumulation. The flow in an ice rise is predominantly radial from a point divide and so we use a radial flux condition

$$\boldsymbol{\nabla} \cdot \boldsymbol{Q} = \frac{1}{R} \frac{\partial}{\partial R}(R Q_R) = \dot{a}_s, \tag{16}$$

~~resulting in an~~ assuming no azimuthal variance. Here, $\mathbf{Q} = Q_R \mathbf{e}_R$ denotes the vertically-integrated flux at a distance R from the origin (located at the ice rise divide). The resulting ice geometry profile is of the form

$$h(R) = h_0 \left[1 - \left(\frac{R}{L} \right)^{\frac{n+1}{n}} \right]^{\frac{n}{2n+2}}, \tag{17}$$

where

$$h_0 = 2^{\frac{n}{2n+2}} \left(\frac{\dot{a}_s}{2A_0}\right)^{\frac{1}{2n+2}} L^{\frac{n+1}{n}} \tag{18}$$

and

$$A_0 = \frac{2A(\rho_i g)^n}{n+2}. \tag{19}$$

~~Both~~ L is the horizontal distance from the ice rise divide to the grounding line, and both h_0 and L are calculated from a reference point on the surface of the full Stokes simulation output.

We compare only the lee profile of the ice rises to the Vialov profile as the bed is relatively flat in this area and we assume that small changes in bed topography are negligible. The profiles are compared for a central cross-section from the divide, extending in the along-flow direction into the ice shelf (Label (~~4~~3) in Fig. 1c).

2.5 Design of transient simulations

To allow perturbation simulations to start from a steady state geometry, all simulations are run for 2000 years under constant forcing. Simulations are performed for three different basal friction coefficients $C = 3.812 \times 10^6$, $C = 7.624 \times 10^6$ and $C = 3.812 \times 10^8$ $\mathrm{Pa\ m^{-1/3}\ s^{1/3}}$, which we will refer to as *low*, *intermediate* and *high* friction scenarios, respectively. The *intermediate* friction scenario has the same basal friction coefficient as that used in MISMIP (Pattyn et al., 2012) and in Favier and Pattyn (2015), where an ice rise is also modelled. The *low* basal friction coefficient is close to the suggested value of 3.16×10^6 $\mathrm{Pa\ m^{-1/3}\ s^{1/3}}$ in MISMIP+ (Cornford et al., 2020). The *high* basal friction scenario essentially excludes basal sliding~~with ice being~~, mimicking ice frozen to the bed. For each basal friction coefficient, transient simulations with variable sea level are performed (Fig. 3). In the *low* and *intermediate* basal friction scenarios, sea level is increased by 80 m at a rate of $0.02\ \mathrm{ma^{-1}}$ over 4000 years and then stays constant for another 2000 years. Sea level is then decreased at a rate of $0.02\ \mathrm{ma^{-1}}$ back to the initial level followed by a second phase of constant sea level for 2000 years. A second cycle is performed for the *low* basal friction scenario for a comparison with the first cycle. Branches of the *low* basal friction simulation are run to steady state (equilibrium) at discrete intervals while keeping sea level fixed. We run these simulation branches in order to understand how far from steady state the transient simulations are. The choice of sea level perturbation rate is in line with observations, showing periods of sea level rise of up to $0.04\ \mathrm{m\ a^{-1}}$ during the last deglaciation (Deschamps et al., 2012). Furthermore, we run branches of the simulation beyond the original sea level at the same sea level decrease rate of 0.02 $\mathrm{m\ a^{-1}}$.

In the *low* and *intermediate* scenarios, the ice rises transition to ice rumples at some stage during the sea level increase. In the high friction scenario, no such transition occurs after a sea level increase of 80 m. We therefore continue the increase of sea level further at a constant rate of $0.02\ \mathrm{m\ a^{-1}}$ until the transition occurs. A reversal of the sea level perturbation is performed from a height of 155 m above the initial sea level.

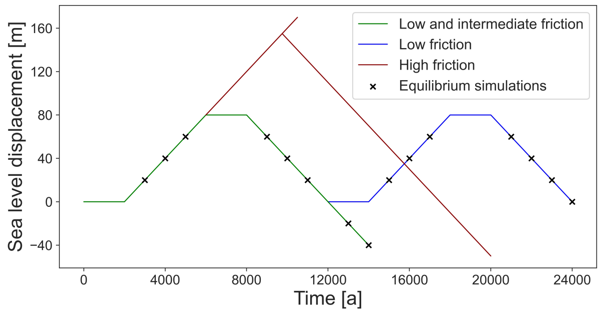

Figure 3. The change in sea level for the transient simulations. The *low* and *intermediate* scenarios follow the green curve. A second sea level increase and decrease cycle is performed for the low friction scenario (blue). Sea level is increased to 170 m in the *high* friction scenario and a separate sea level decrease branch is simulated from 155 m (red curve). Sea level is increased and decreased at rates of $\pm 0.02\ \mathrm{ma}^{-1}$. The crosses indicate points in the *low* friction scenario at which a steady state branch is started with constant sea level in order to compare to the transient simulation.

3 Results

3.1 Steady state analysis before sea level perturbation

After 2000 years of spin-up time, ice rises with a characteristic local flow regime develop in all three full Stokes scenarios (Fig. 4). From low to high friction, they vary in maximum thickness ($H_{max} = 213 - 468\ \mathrm{m}$), grounded area ($132 - 225\ \mathrm{km}^2$), and characteristic timescale ($t_c = 178 - 391\ \mathrm{a}$, defined as $t_c = H_{max}/\dot{a_s}$). The characteristic timescale is a metric that gives an indication of the rate of development of Raymond arches (Martín et al., 2009; Goel et al., 2020). The ice divide position in the *high* friction scenario has a stossward offset of $0.9\ \mathrm{km}$ from the vertical symmetry axis of the bed protrusion. In the *intermediate* and *low* friction scenarios it is shifted stossward by 2.7 and $3.3\ \mathrm{km}$, respectively. In all three cases, there is substantially more grounding on the stoss side of the bed protrusion than on the lee side.

Topographic and flow divides coincide in all three cases, and ice rise surface velocities are within tens of metres per year. There is negligible basal sliding in the high friction scenario (with average absolute velocities of roughly $0.5 \times 10^{-4}\ \mathrm{m\ a}^{-1}$ at the bed-ice interface), whereas basal sliding in the along-flow cross-section (Label (43) in Fig. 1c) accounts for 90 % and 98 % of the local mean horizontal velocities in the *intermediate* and *low* friction scenarios, respectively. The width of the lateral shear zones, here defined as the lateral distance from the grounding line along a cross-section (Label (2) in Fig. 1c) in which v_x reaches 90 % of v_x at the domain boundary, vary marginally from 10 to $11.3\ \mathrm{km}$ from the *low* to the *high* friction scenarios. Ice fluxes upstream of the protrusion are approximately equal, but mean velocities are 15 % slower and ice is about 15 % thicker in the *high* friction scenario compared with the *low* friction scenario.

All ice rises exhibit geometries and flow regimes which are comparable to observations. For example, the *high* friction scenario is comparable to Derwael Ice Rise, where previous studies have assumed no basal sliding a priori (e.g. Drews et al.

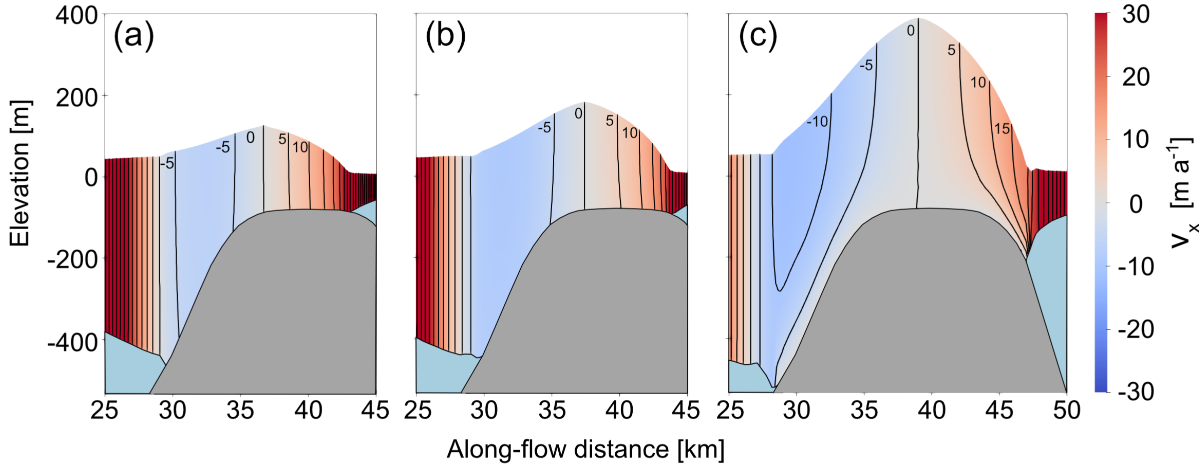

Figure 4. A cross-section of the ice rise in the along-flow direction for (a) the low basal friction, (b) the intermediate basal friction and (c) the high basal friction scenarios. The contours show lines of equal velocity (full Stokes) in the x-direction~~(~~, i.e. in the along-flow direction~~)~~.

(2015)). Basal sliding in the *low* and *intermediate* basal friction scenarios means these ice rises are more susceptible to transition into ice rumples when sea level is raised, as shown later.

3.2 ~~The influence of the surrounding ice shelves on the local flow regime of ice rises~~

The comparison of full Stokes surface velocities to SIA surface velocities on ice rises illustrates where the local flow assumptions are violated. Fig. 5 shows that all three basal friction scenarios have mismatches near the ice rise divides where longitudinal stress gradients are significant. The *high* basal friction scenario shows a good fit otherwise, as do the *low* and *intermediate* basal friction scenarios on the lee sides. However, for these cases, surface velocities differ more on the stoss sides of the ice rises (Fig. 6). In the *low* friction scenario, absolute deviations increase from 0-20 % in the vicinity of the divide (but not at the divide), to over 100 % closer to the grounding line. In the *intermediate* friction scenario, deviations are not quite as significant, but nonetheless reach a ~~maximum deviation a of 80~~ deviations of 100 %. In terms of ice thickness, the Vialov approximation captures the *high* friction scenario well despite the non-flat bed, while it significantly overestimates the *low* and *intermediate* ~~friction scenario~~ basal friction scenarios in which basal sliding is dominant (Fig. 7).

3.2 Ice rise to ice rumple transitions triggered by sea level variation

To understand the response of ice rises and ice rumples with differing basal friction to sea level perturbation, we analyse the grounded area (Figs. 8a,b and 9a), dome migration (Fig. 10), lee side grounding line position ~~as well as~~ and the upstream ice shelf velocities (Figs. 8c,d and 9b). The upstream ice shelf velocity is defined as the mean velocity of ice in the x-direction at $x = 20$ km, as marked by Label (1) in Fig. 1c. In terms of these metrics, the *low* and *intermediate* basal friction scenarios behave distinctly different than the *high* basal friction scenario. The former transition gradually to ice rumples if sea level is

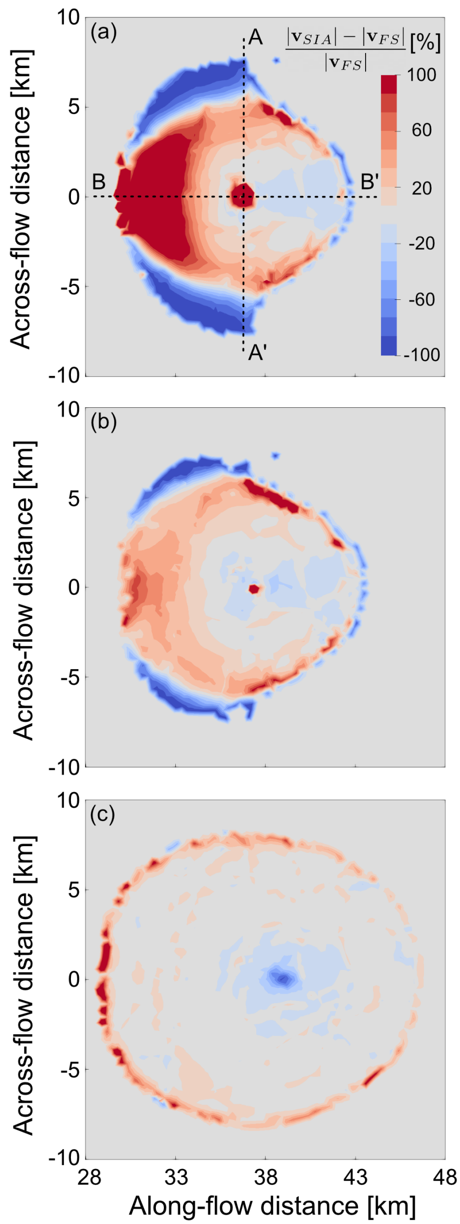

Figure 5. A bird's eye view of the grounded area corresponding to the steady states at $t = 2000$ years of the simulations with (a) a *low* basal friction, (b) an *intermediate* basal friction and (c) a *high* basal friction. In colour, the percentage difference is shown between the calculated SIA surface velocity magnitude and the full Stokes velocity magnitude.

raised past a certain threshold and regrow into ice rises if sea level is reversed. The reversal is not symmetric and the respective steady state geometries depend on the history of their evolution (i.e. hysteresis). The *high* basal friction scenario, on the other hand, requires a much larger sea level perturbation to trigger transition into an ice rumple. Once this transition is reached, an

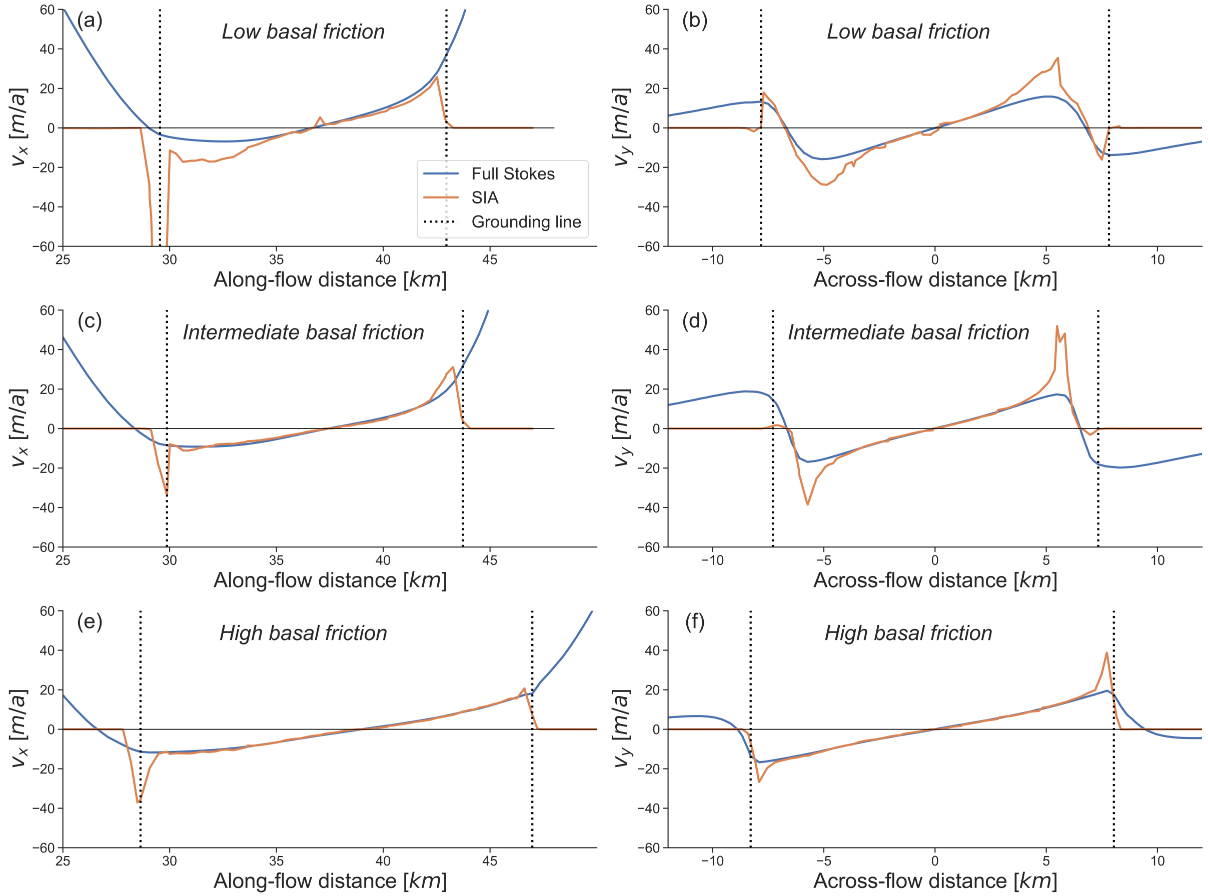

Figure 6. The full Stokes and SIA surface velocities at $t = 2000$ years in the along-flow direction ((a), (c) and (e)), and in the across-flow direction ((b), (d) and (f)), as indicated by the cross-sections A-A' and B-B' through the divide in Fig. 5. Figures (a) and (b) show the *low* basal friction scenario, (c) and (d) show the *intermediate* basal friction scenario, and (e) and (f) show the *high* basal friction scenario.

ice rumple forms but the system is unstable and the ice rumple ungrounds entirely. Details of these differing states are provided in the following.

Before transitioning to an ice rumple, the dome position in the *low* friction scenario migrates linearly at a rate of 1.7 m a^{-1} with increasing sea level (Fig. 10). The dome of the *intermediate* friction ice rise migrates first at a rate of 0.8 m a^{-1} before increasing to a migration rate of 5.7 m a^{-1} after a sea level increase of 29 m. The dome of the *high* basal friction ice rise exhibits a slow response to sea level displacement during the first 152 m of sea level increase with a divide migration rate of 0.2 m a^{-1}, before increasing to a migration rate of 5.0 m a^{-1}.

After a sea level increase of 20 m in the case of the *low* friction case, 30 m in the case of the *intermediate* friction case, and 161 m in the high friction case, the grounding line on the lee side of the ice rise migrates past the highest point of the bed anomaly (marked by A in Fig. 1e), and so, is located on a retrograde slope. A transition from ice rise to ice rumple occurs

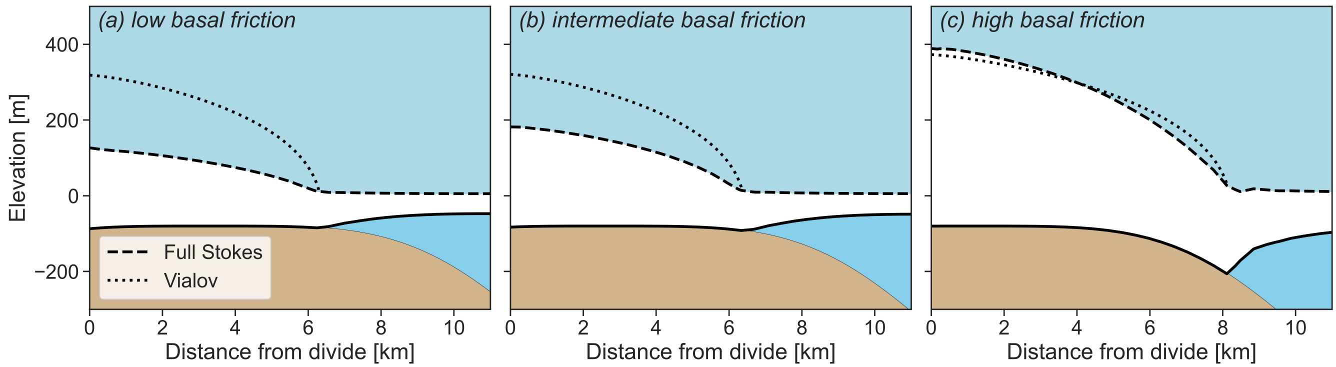

Figure 7. Cross-sections of the full Stokes simulations at $t = 2000$ years in the case of the (a) *low* basal friction coefficient, (b) the *intermediate* and (c) the *high* basal friction coefficient. Using a reference point on the ice surface at the grounding line, a Vialov profile is calculated and plotted.

at a further sea level displacement of 30, 16 and $1\ \mathrm{m}$ after the grounding line has reached this point in the case of the *low*, *intermediate* and *high* basal friction scenarios, respectively.

A steady acceleration of the upstream ice shelf is seen in both the *low* and *intermediate* basal friction scenarios and there is no abrupt change once a transition from ice rise to ice rumple has occurred (Fig. 8). This is in contrast to the *high* basal friction scenario, where there is an abrupt change in the upstream ice shelf velocity as a transition from ice rise to ice rumple is approached.

After keeping the sea level constant for 2000 years at a sea level perturbation of 80 m, the *low* and *intermediate* basal friction ice rumples evolve to their respective steady states, with minimum velocities of 20 and $38\ \mathrm{m\ a^{-1}}$ (Fig. 12). Reversal of the sea level perturbation then triggers an asymmetric reversal of the variables of interest described above, with grounded area and upstream ice shelf thickness increasing and upstream velocity decreasing. A transition from ice rumple to ice rise (Figs. 8 and A1) is observed ~~at sea level displacements of~~ when sea level is 21 and $19\ \mathrm{m}$ ~~from~~ above the initial sea level in the *low* and *intermediate* basal friction scenarios, respectively (as opposed to displacements of 50 and $45\ \mathrm{m}$ for *low* and *intermediate* basal friction scenarios in the sea level increase scenarios, respectively). Once the original sea level is again reached, the ice rises in both the *low* and *intermediate* basal friction scenarios are smaller, with a smaller grounded area and a lesser buttressing effect on the upstream ice shelf (Figs. 8, A1 and 11). The upstream ice shelf in the case of the *low* basal friction scenario has a decrease in velocity of $18\ \mathrm{m\ a^{-1}}$ whereas the ice shelf in the *intermediate* decreases in velocity by $25\ \mathrm{m\ a^{-1}}$. A second cycle of sea level increase and decrease is performed for the *low* basal friction scenario starting from the steady states that emerged from the previous sea level perturbation cycle. The response of the grounded area ~~,~~ and ice shelf velocity ~~and thickness~~ are calculated as described above ~~(~~and presented in Fig. 8~~)~~. The hysteresis ~~cycles are now closedand independent of the initial conditions~~cycle is now closed, with the final steady state corresponding to the state before the last sea level perturbation cycle.

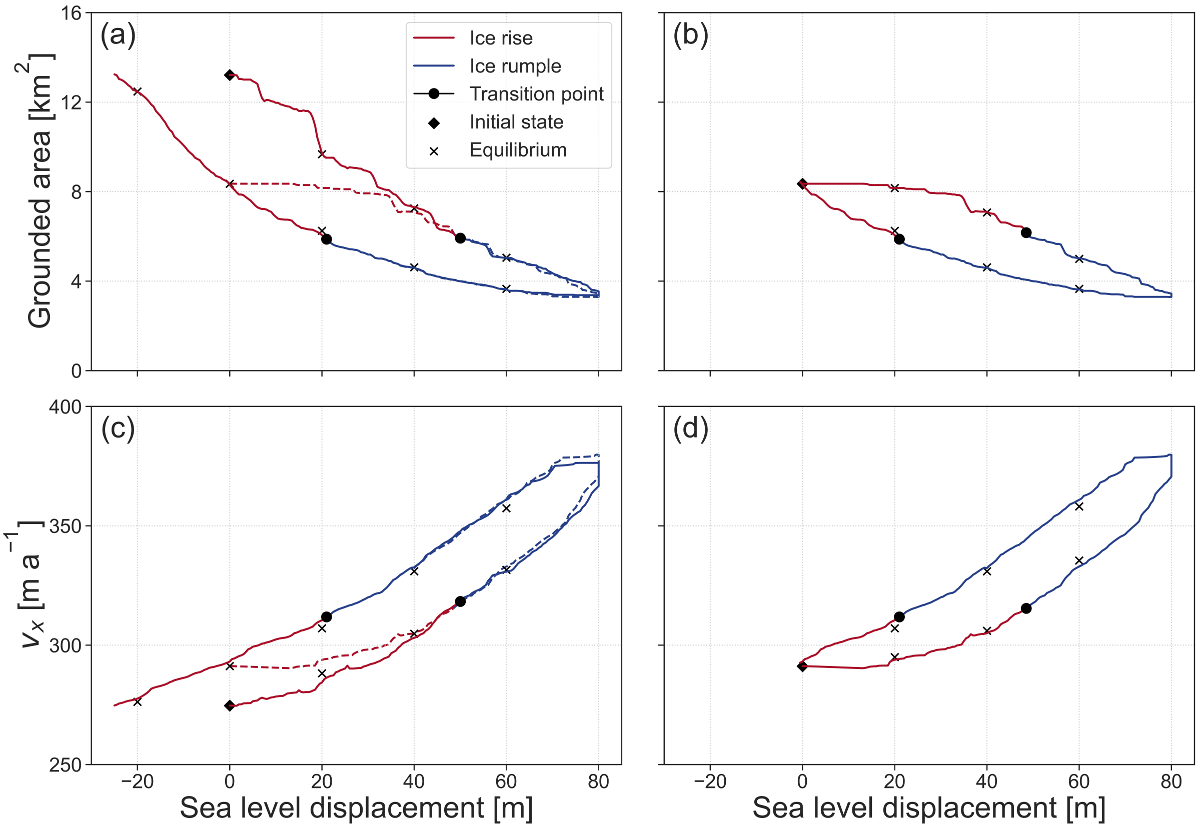

Figure 8. The response of grounded area and upstream ice shelf velocity to sea level perturbation in the case of the *low* basal friction. Panels (a) and (c) show the evolution for the first sea level increase and decrease cycle in blue and red. Panels (b) and (d) show the evolution for the second increase and decrease cycle. These curves are also plotted in panels (a) and (c) in with dashed red and blue lines for comparison. The crosses represent the results of steady state branches of the transient simulations at corresponding sea levels. The transition from ice rise to rumple and vice versa is represented by the black dots and a change in colour of the curve.

When sea level rise is halted in the *high* basal friction scenario prior to the unstable grounding line retreat (here at a sea level perturbation of 155 m), ~~then~~ the ice rise volume and grounded area also recover asymmetrically resulting in two ~~viable~~ differing states for a given sea level displacement (Fig. 9).

We investigate the migration of the stoss and lee side grounding lines of the ice rise and make a comparison with the grounding line position in the case of hydrostatic equilibrium (supplementary video). The maximum differences in position are 0.5 km on the stoss side and 0.4 km on the lee side, with mean differences of 0.2 km in both cases. During sea level increase, the hydrostatic grounding line positions have a delayed response in comparison with the Elmer/Ice grounding line. On the other hand, during sea level decrease, the hydrostatic grounding lines have a more rapid response.

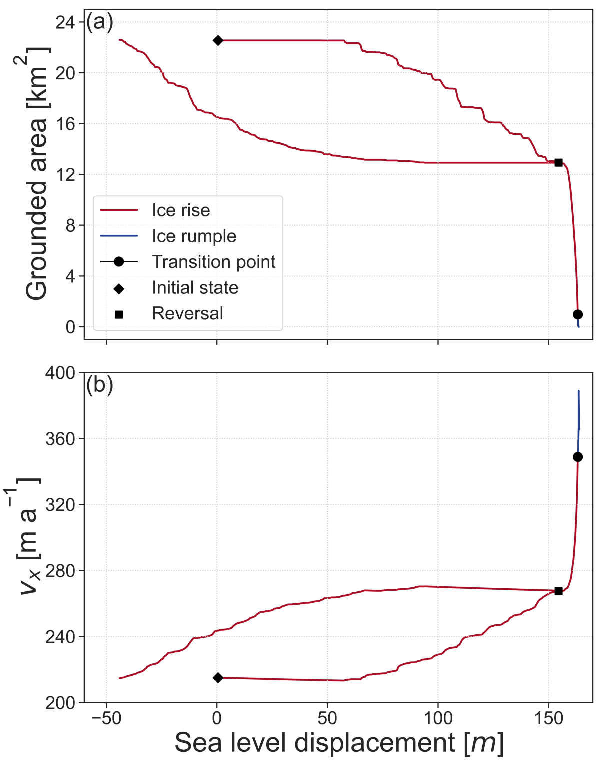

Figure 9. The response of grounded area and upstream ice shelf velocity to sea level perturbation in the case of the *high* basal friction. In (a), the grounded area is plotted against sea level displacement and in (b), the average velocity in the x-direction in a cross-section upstream of the ice rise (at 20 km from the influx boundary). Red indicates that the system exhibits a characteristic flow regime of an ice rise and blue indicates that of an ice rumple. The square indicates from where a reversal of the sea level perturbation is simulated.

4 Discussion

4.1 The influence of basal sliding on the geometry and transient behavior of ice rises

A number of previous studies have argued that basal sliding near ice rise divides is negligible because thermomechanically coupled models often predict ice significantly below freezing point at the ice-bed interface near the summits (Martín et al., 2009; Drews et al., 2015; Goel et al., 2020) and because many ice rises exhibit isochronal features called Raymond arches which do not form if basal sliding is dominant (Pettit et al., 2003; Martín et al., 2009). However, *low* and *intermediate* scenarios can be relevant in areas where Holocene marine sedimentation results in basal sliding in areas which have regrounded (Pollard et al., 2016). Moreover, differences between observed and simulated Raymond arches under a frozen bed assumption may indicate a delay or suppression of arch growth due to past or present basal sliding (Kingslake et al., 2016).

The simulations show that ice rises can form in scenarios where basal sliding is significant. Surface velocities in the *low* and *intermediate* scenarios are within a few meters per years near the crests, similar to the predictions in the *high* friction scenario

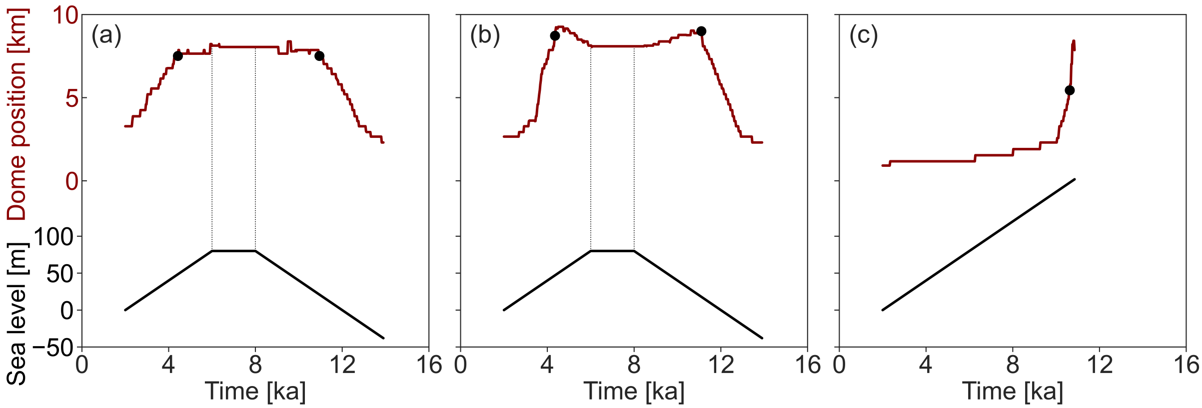

Figure 10. The response of the dome position to a raising and lowering of sea level in the case of (a) the low, (b) the intermediate and (c) the high basal friction coefficients.

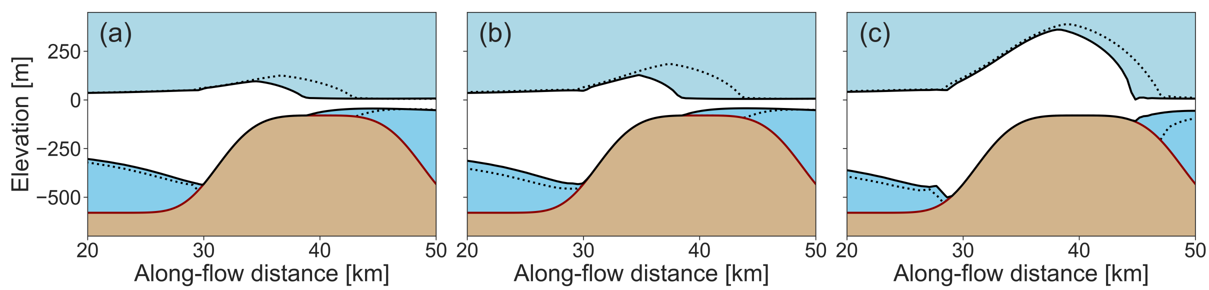

Figure 11. The figures show a cross-section of the ice rises in the along-flow direction for (a) the *low*, (b) the *intermediate* and (c) the *high* basal friction scenario. The dotted lines show the geometry of the ice rises before sea level perturbation and the ~~blue~~ solid lines show the geometry after ~~an equal~~ a full cycle of sea level increase and decrease~~in sea level~~.

(Fig. 5). In this regard, surface velocities alone are a poor indicator for the presence or absence of basal sliding on ice rises. However, the geometries between the three scenarios differ significantly, and only the high friction scenario can be adequately approximated with the Vialov profile whereas the *low* and *intermediate* scenarios exhibit significant misfits (Fig. 8). This means that a simple fit with a Vialov profile can serve as a first order metric for absence or existing of basal sliding for specific ice rises. This is important, as the degree of basal sliding in the vicinity of the grounding line determines the local ice flow and the ice rise's transient behaviour in response to sea level perturbation. When comparing the ~~ad hoc~~ grounding line positions of the full Stokes model and the hydrostatic grounding line position, we find that differences are small. However, over the millennial timescales considered here, together with the compounding effect of the small errors in grounding line position at each time step, it is possible that a hydrostatic assumption may result in differing ice rise and ice rumple geometries as well as a differing transition point.

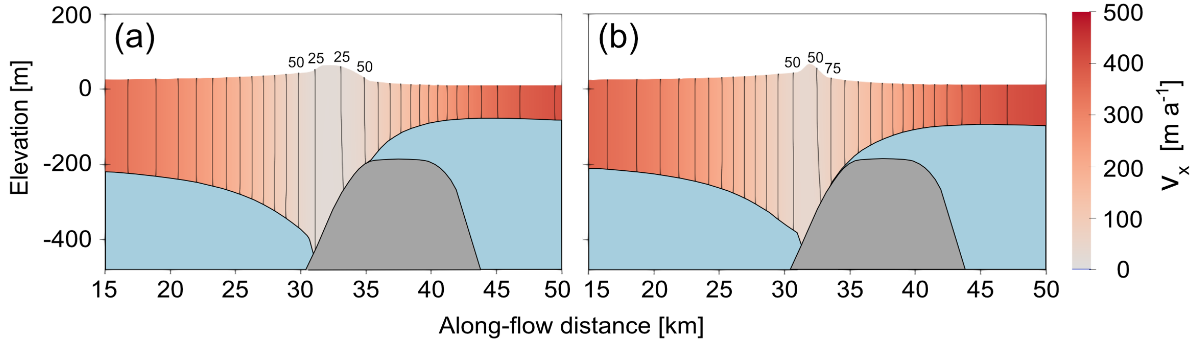

Figure 12. An along-flow cross-section of the ice rumple at $t = 8000$ years in the case of (a) the low basal friction and (b) the ~~high~~ intermediate basal friction. The contours show lines of equal velocity in the x-direction and are spaced $25\ \mathrm{m\ a^{-1}}$ apart.

Many ice rises are fully surrounded by ice shelves and the extent to which isle-type ice rise velocities are affected by longitudinal and shear stresses transferred from the upstream ice shelf is not fully clear. This effect is analysed here using the differences between the non-local full Stokes simulations and the fully local SIA. The flow regime in the *high* friction scenario is, to a large extent, independent of the surrounding ice shelf. In the *low* and *intermediate* basal friction scenarios, however, the differences between full Stokes and SIA are greater, and are especially evident on the stoss side of the ice rise. The greater velocity differences in the lower friction scenarios show that these ice rises are influenced more by the stresses in the surrounding ice shelf. Implications for the presence or absence of a fully local flow regime are twofold: (1) if basal sliding is negligible even in areas close to the grounding zone, then SIA is an appropriate modelling framework, for example, when investigating the surface accumulation history using inverse methods (Callens et al., 2016), and (2) the basal boundary condition determines an ice rise's response to sea level perturbation.

The *low* and *intermediate* friction scenarios respond immediately to a rising sea level, with a retreat of the leeward grounding line accompanied by a stossward migration of the dome position. The ice rises progressively thin and eventually transition into ice rumples. There is no significant threshold behaviour between these two states and once the sea level increase is halted, the system converges to a steady state ice rumple with the lee side grounding line located on the retrograde slope at the edge of the basal plateau. The summits are a few tens of meters above the ice shelf surface and the overall geometry is consistent with, for example, the ice rumple located in the Roi Baudouin Ice Shelf (Fig. 13). The minimum overriding velocities of $20\ \mathrm{m\ a^{-1}}$ are, however, significantly faster than the example observed at the Roi Baudouin Ice Shelf where the ice is effectively stagnant (Berger et al., 2016). The smooth transition of the *low* and *intermediate* friction ice rises into ice rumples reflects their strong coupling to the surrounding ice shelf, highlighted previously. From a larger scale perspective there are no critical differences between ice rises and ice rumples in those scenarios other than the switch from a local to an overriding flow regime.

Conversely, the *high* friction case only transitions to an ice rumple for sea level perturbations that are greater than what is expected in a glacial-interglacial cycle. In fact, there is no noticeable change in grounded area even for a sea level displacement

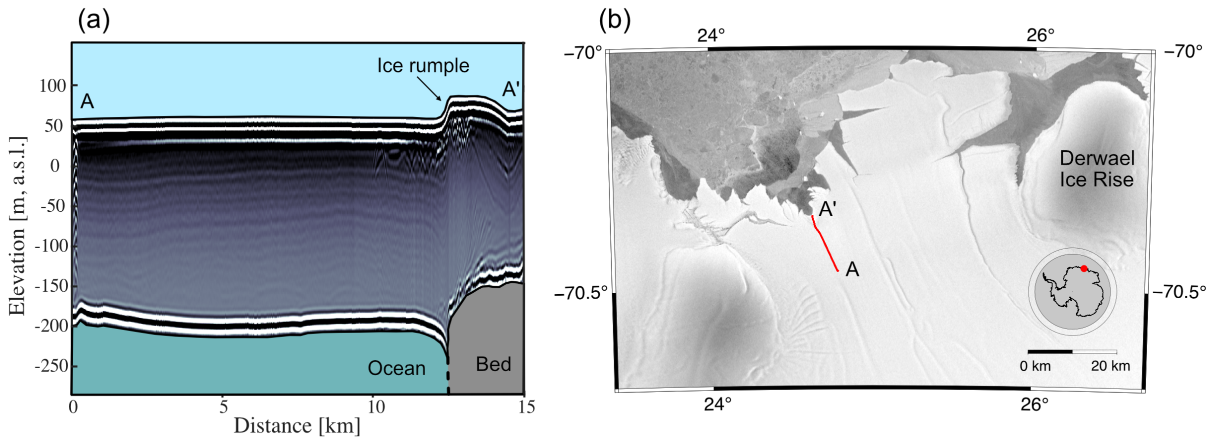

Figure 13. An along-flow ground-based radargram (Drews, 2019) showing an ice rumple in the Roi Baudouin Ice Shelf, East Antarctica is shown in (a). The flow of ice is from left (A) to right (A'). In (b), the location of the radargram (A-A') is shown (Jezek, 2003).

of 50 m. This stability is in line with, for example, ice promontories at the Ekström Ice Shelf which show a comparatively weak response to the thinning of their surrounding ice shelves (Schannwell et al., 2019). Grounding line retreat rates for higher sea level displacements then remain moderate as long as the leeward side remains grounded on a prograde slope. On a retrograde slope the ice rise becomes unstable and complete ungrounding occurs. We therefore conclude that after a transition from ice rise, there is a threshold basal friction beyond which a steady state ice rumple cannot form.

Interestingly, the *low* friction ice rumple exhibits lower minimum velocities than the *intermediate* friction ice rumple, most likely due to a greater grounded area (Fig. 12) and it is worth investigating whether inverse techniques used to predict the basal friction coefficient beneath pinning points produce results which remain valid regardless of ~~the~~ horizontal resolution and changes in grounded area.

The required sea level perturbation for ungrounding clearly depends on the elevation below sea level of the bed protrusion, but the scenarios shown here with a maximum bed elevation of 80 m below sea level have many real world counterparts (e.g., Kupol Moskovskij, Kupol Coilkovskogo, Leningrad Ice Rise, Djupranen Ice Rise (Goel et al., 2020), Derwael Ice Rise (Drews et al., 2015)). Our study suggests that features with a high basal friction have been and will remain stable local flow features even for comparatively large sea level perturbations. Moreover, it shows that ice rumples with comparatively low surface velocities as in the example provided in Fig. 13, are very unlikely a result of a deglaciated ice rise. An area that requires more investigation is the case of ice rises which do not conform to the plateau-shaped bed topography as prescribed here. The unstable retreat predicted in the high basal friction scenario suggests that ice rises located on retrograde slopes are critically less stable for an equal amount of sea level displacement.

4.2 The hysteretic behaviour of ice rises over glacial cycles

In all basal friction scenarios, there are two differing ice rises for a given sea level (Figs. 8, 9). These pairs differ in the basal melt rate applied (which is thickness dependent) and in the grounded area. Each pair corresponds to a low and a high buttressing case for which the averaged upstream ice velocity is used as a proxy (Figs. 8c,d, 9b and Fig. A1b in the Appendix).

~~The differences in grounded area occupied for~~ There is a difference in the individual pairs~~is asymmetric~~, with the grounded area being larger in the sea level increase scenario than in the sea level decrease scenario. In all cases, the pairs occupy virtually the same region on the obstacle's stoss side, but the extent of grounding on the plateau differs (Fig. 11). The thickness and slopes at the respective grounding lines are comparable, and therefore differences in basal melt (as parameterised in Eq. 8) are small, with differences of only 3.5, 3.0 and 2.4 % in the *low*, *intermediate* and *high* friction scenarios, respectively. The dynamic differences therefore stem mostly from the differing grounded areas that result in a differing form drag (Still et al., 2019) and consequently a differing net resistance to the upstream ice shelf.

A ~~relevant~~ self-stabilising feedback occurs, ~~whereby the~~ with divide migration opposing grounding line retreat in a sea level increase scenario. The ice rise height reduces and the divide migrates stossward during lee side grounding line retreat. ~~This increases the lee side accumulation area in the vicinity of the dome, thereby increasing the ice flux~~ Because the divide moves stossward, the area of accumulation adjacent to the divide on the lee side ~~and slowing the grounding line retreat. In the same way~~of the ice rise increases. The increased accumulation area promotes an increased flux across the grounding line, opposing grounding line retreat. Analogously, sea level decrease results in leeward divide migration~~, slowing the~~ . The resulting reduction in accumulation area adjacent to the divide on the lee side of the ice rise opposes grounding line advance. The existence of negative feedback mechanisms in both the sea level increase and decrease scenario result in hysteretic behaviour (Figs. 8, 9, A1).

Another mechanism that plays a role is the sensitivity of the grounding line to bed shape, with hysteretic behaviour occurring due to the positioning of retrograde and prograde slope segments (Schoof, 2007; Pattyn et al., 2012; Haseloff and Sergienko, 2018; Sergienko and Wingham, 2022). In our study, we also observe grounding line migration patterns linked to the shape of the three-dimensional bed protrusion. Consequently, it matters how the ice rise and ice rumple geometries are initialised to begin with.

Although in our study, we have used a constant surface accumulation, we would expect orographic precipitation to enhance the hysteretic behaviour. In future work it is worth investigating whether effects such as an increased melt rate also produce an hysteretic response in ice rises and ice rumples. Given that the grounded area and basal sliding determine the ice rise evolution, future simulations should include a more informative guess of the basal friction coefficients guided by, for example, seismic studies determining the bed properties (Smith et al., 2015). Inversion of the basal friction parameters from a thermo-mechanically coupled full Stokes model (Schannwell et al., 2019, 2020) does provide some information in this regard, but also contains lumped uncertainties, e.g., from ice rheology and uncertain boundary conditions. Another process not considered here is changes in the bed protrusion through glacial isostatic adjustment (Kingslake et al., 2018; Wearing and Kingslake, 2019).

The existence of multiple steady states means that the grounding lines of ice rises and ice rumples observed today are dependent on the local ice flow history during the last glacial cycle. Inversely, the dynamics and buttressing effect of ice rises and ice rumples are dependent on the initial geometry prescribed, which is typically unknown. The degree of buttressing is of importance for determining the stability and evolution of the continental grounding line (Favier and Pattyn, 2015; Reese et al., 2018). The representation of ice shelves has been identified as a key cause of continental-scale model spread (Seroussi et al., 2019) and a precise representation of ice rises and ice rumples would reduce spin-up and projection uncertainties.

We have shown that the difference between the simulated grounding line and the hydrostatic equilibrium grounding line is small at each time step. This small error may, however, lead to an error propogation during transient simulation leading to inaccurate grounding line migration if a hydrostatic equilibrium assumption is used.

5 Conclusions

We examined the effect of basal friction and sea level variation on the evolution of ice rises and ice rumples using idealised simulations including the surrounding ice shelves. In a high basal friction scenario, there is negligible mismatch when comparing simulated steady state full Stokes velocities with steady state SIA velocities, whereas in a low basal friction scenario the mismatch is larger due to ~~a greater influence of stresses from~~ stronger mechanical coupling to the surrounding ice shelf. The locality of the ice flow and the degree of basal sliding can be diagnosed by examining the (mis-)fit of a Vialov profile to the observed thickness profile. In response to an increasing sea level, a transition from ice rise to ice rumple occurs. Steady state ice rumples form in the low basal friction scenarios whereas the ice rumple in the high friction scenario is ephemeral and ungrounds rapidly. The higher friction ice rise, on the other hand, is largely unresponsive to sea level variations, requiring more than double the sea level rise to trigger the transition compared to the lower friction scenarios.

All basal friction scenarios show self-stabilising, hysteretic behaviour, with grounded area and upstream ice shelf buttressing dependent on the evolution history. As a consequence of this behaviour, we identify the ~~need for careful consideration of~~ importance of perturbation history for the formation of the ~~grounded area of an ice rise during model initialisation in order for the~~ correct feature~~to form~~. Although in our study, we have concentrated only on the response of ice rises to sea level perturbation, further processes such as an increase in basal melt are also likely to result in hysteretic and potentially irreversible behaviour in ice shelf buttressing upstream of ice rises.

Code availability. The code used to run the simulations and the post-processing code can be found at https://doi.org/10.5281/zenodo.6355565. The Elmer version is Version: 8.4 (Rev: 1c584234)

Video supplement. A supplementary video is provided, showing the evolution of an ice rise in response to sea level perturbation as well as the position of the grounding line if the system were in hydrostatic equilibrium.

Appendix A: The response of the grounded area and ice shelf velocity to sea level perturbation in the *intermediate* basal friction scenario.

Presented in Fig. A1 is the response of the grounded area and upstream velocity to sea level perturbation in the case of the *intermediate* ($C = 7.624 \times 10^6$ $\mathrm{Pa\,m^{-1/3}\,s^{1/3}}$) basal friction scenario. The transition from ice rise to ice rumple occurs at a sea level displacement of 19 m and the transition from ice rumple to ice rise occurs at a sea level displacement of 45 m, compared with 21 m and 50 m, respectively, in the *low* basal friction scenario). Interestingly, the grounded area of the ice rumple follows a rather linear path in the *intermediate* basal friction scenario compared with the *low* basal friction scenario.

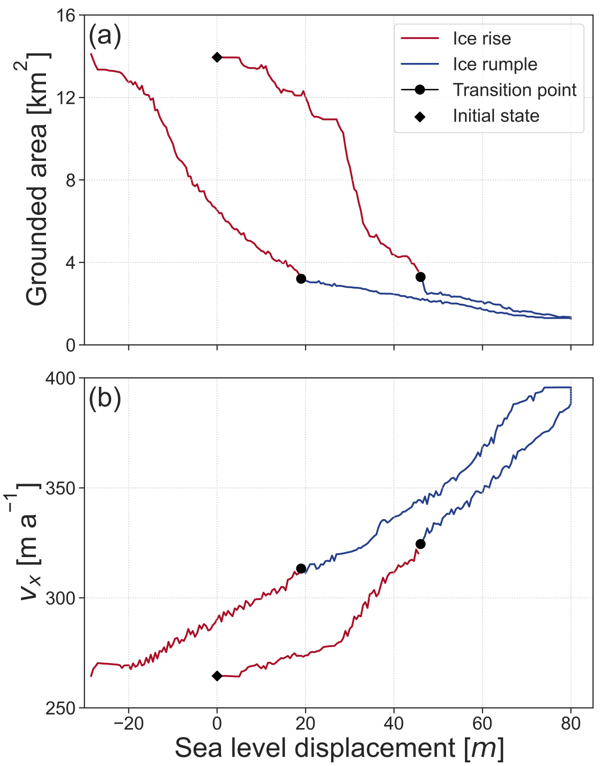

Figure A1. The response of the grounded area and ice shelf velocity to sea level perturbation in the *intermediate* friction scenario. In (a), the grounded area is plotted against sea level displacement and in (b), the average velocity in the x-direction in a cross-section upstream of the ice rise (at 20 km from the influx boundary). Red indicates that the system exhibits a characteristic flow regime of an ice rise and blue indicates that of an ice rumple.

A1

Appendix B: Comparison between the *First Floating* and *Discontinuous* grounding line numerical implementations

In the case of the *low* basal friction scenario, we have run equivalent simulations using a differing grounding line numerical implementation, namely the *Discontinuous* method (Fig. B1). At the grounding line, basal friction is applied if the other two nodes in the element are also grounded and a free-slip condition is applied if the other two nodes are ungrounded. The *First Floating* numerical implementation, however, assumes a free-slip condition at the grounding line and a linear reduction in basal friction between it and the upstream node is applied. Although the *Discontinuous* numerical implementation has been shown to have the least dependence on mesh resolution, it can be argued that the *First Floating* is more plausible physically, with effective pressure disappearing at the grounding line (Gagliardini et al., 2016). The simulations show that regardless of the numerical implementation, hysteresis occurs.

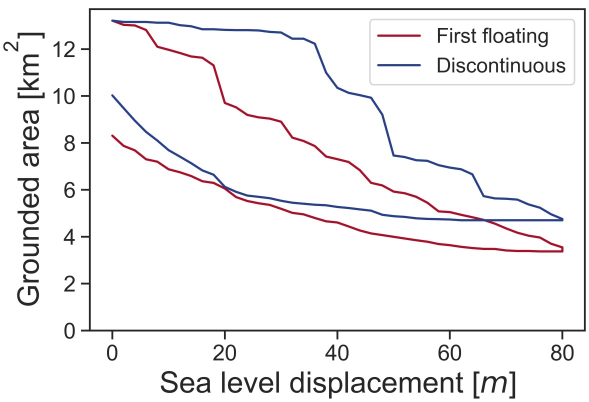

Figure B1. Shown is the response of the grounded area in the low friction case of the *First Floating* (red) and *Discontinuous* (blue) Elmer/Ice numerical grounding line implementations.

Author contributions. C. Henry, C. Schannwell, and R. Drews conceived the idea for the study and designed the experiments. C. Henry performed the simulations and analysis. The manuscript was written by C. Henry with contributions from all authors.

Competing interests. R. Drews is an editor for The Cryosphere.

Acknowledgements. C. Henry was supported by the Deutsche Forschungsgemeinschaft (DFG) in the framework of the priority programme 1158 "Antarctic Research with comparative investigations in Arctic ice areas" by a grant SCHA 2139/1-1. C. Schannwell was supported by the German Federal Ministry of Education and Research (BMBF) as a Research for Sustainability initiative (FONA) through the PalMod project under the grant number 01LP1915C. R. Drews and V. Višnjević were supported by an Emmy Noether Grant of the Deutsche Forschungsgemeinschaft (DR 822/3-1). This work used resources of the Deutsches Klimarechenzentrum (DKRZ) granted by its Scientific Steering Committee (WLA) under project ID bm1164. The authors gratefully acknowledge the Gauss Centre for Supercomputing e.V.

(www.gauss-centre.eu) for funding this project by providing computing time on the GCS Supercomputer SuperMUC-NG at Leibniz Supercomputing Centre (www.lrz.de). Data for Fig. 13 were collected with the support of the InBev Baillet Latour Antarctica Fellowship with logistic support from the International Polar Foundation.

References

MMG Platform, http://www.mmgtools.org/,version5.3.10, accessed: 17-06-2022.

Albrecht, T., Winkelmann, R., and Levermann, A.: Glacial-cycle simulations of the Antarctic Ice Sheet with the Parallel Ice Sheet Model (PISM) – Part 1: Boundary conditions and climatic forcing, The Cryosphere, 14, 599–632, https://doi.org/10.5194/tc-14-599-2020, 2020.

Barletta, V. R., Bevis, M., Smith, B. E., Wilson, T., Brown, A., Bordoni, A., Willis, M., Khan, S. A., Rovira-Navarro, M., Dalziel, I., Smalley, R., Kendrick, E., Konfal, S., Caccamise, D. J., Aster, R. C., Nyblade, A., and Wiens, D. A.: Observed rapid bedrock uplift in Amundsen Sea Embayment promotes ice-sheet stability, Science, 360, 1335–1339, https://doi.org/10.1126/science.aao1447, 2018.

Berger, S., Favier, L., Drews, R., Derwael, J.-J., and Pattyn, F.: The control of an uncharted pinning point on the flow of an Antarctic ice shelf, Journal of Glaciology, 62, 37–45, https://doi.org/10.1017/jog.2016.7, 2016.

Bindschadler, R., Vornberger, P., and Gray, L.: Changes in the ice plain of Whillans Ice Stream, West Antarctica, Journal of Glaciology, 51, 620–636, https://doi.org/10.3189/172756505781829070, 2005.

Bindschadler, R. A., Roberts, E. P., and Iken, A.: Age of Crary Ice Rise, Antarctica, Determined from Temperature-Depth Profiles, Annals of Glaciology, 14, 13–16, https://doi.org/10.1017/S0260305500008168, 1990.

Callens, D., Drews, R., Witrant, E., Philippe, M., and Pattyn, F.: Temporally stable surface mass balance asymmetry across an ice rise derived from radar internal reflection horizons through inverse modeling, Journal of Glaciology, 62, 525–534, https://doi.org/10.1017/jog.2016.41, 2016.

Cornford, S. L., Martin, D. F., Lee, V., Payne, A. J., and Ng, E. G.: Adaptive mesh refinement versus subgrid friction interpolation in simulations of Antarctic ice dynamics, Annals of Glaciology, 57, 1–9, https://doi.org/10.1017/aog.2016.13, 2016.

Cornford, S. L., Seroussi, H., Asay-Davis, X. S., Gudmundsson, G. H., Arthern, R., Borstad, C., Christmann, J., Dias dos Santos, T., Feldmann, J., Goldberg, D., Hoffman, M. J., Humbert, A., Kleiner, T., Leguy, G., Lipscomb, W. H., Merino, N., Durand, G., Morlighem, M., Pollard, D., Rückamp, M., Williams, C. R., and Yu, H.: Results of the third Marine Ice Sheet Model Intercomparison Project (MISMIP+), The Cryosphere, 14, 2283–2301, https://doi.org/10.5194/tc-14-2283-2020, 2020.

Deschamps, P., Durand, N., Bard, E., Hamelin, B., Camoin, G., Thomas, A. L., Henderson, G. M., Okuno, J., and Yokoyama, Y.: Ice-sheet collapse and sea-level rise at the Bølling warming 14,600 years ago, Nature, 483, 559–564, https://doi.org/10.1038/nature10902, 2012.

Drews, R.: Ice thickness, surface-, and bed elevation of a pinning point in Roi Baudouin Ice Shelf, Dronning Maud Land Antarctica, https://doi.org/10.1594/PANGAEA.905997, supplement to: Berger, Sophie; Favier, Lionel; Drews, Reinhard; Derwael, Jean-Jacques; Pattyn, Frank (2016): The control of an uncharted pinning point on the flow of an Antarctic ice shelf. Journal of Glaciology, 62(231), 37-45, https://doi.org/10.1017/jog.2016.7, 2019.

Drews, R., Martín, C., Steinhage, D., and Eisen, O.: Characterizing the glaciological conditions at Halvfarryggen ice dome, Dronning Maud Land, Antarctica, Journal of Glaciology, 59, 9–20, https://doi.org/10.3189/2013JoG12J134, 2013.

Drews, R., Matsuoka, K., Martín, C., Callens, D., Bergeot, N., and Pattyn, F.: Evolution of Derwael Ice Rise in Dronning Maud Land, Antarctica, over the last millennia, Journal of Geophysical Research: Earth Surface, 120, 564–579, https://doi.org/10.1002/2014JF003246, 2015.

Durand, G., Gagliardini, O., de Fleurian, B., Zwinger, T., and Le Meur, E.: Marine ice sheet dynamics: Hysteresis and neutral equilibrium, Journal of Geophysical Research, 114, F03 009, https://doi.org/10.1029/2008JF001170, 2009.

Favier, L. and Pattyn, F.: Antarctic ice rise formation, evolution, and stability, Geophysical Research Letters, 42, 4456–4463, https://doi.org/10.1002/2015GL064195, 2015.

Favier, L., Gagliardini, O., Durand, G., and Zwinger, T.: A three-dimensional full Stokes model of the grounding line dynamics: effect of a pinning point beneath the ice shelf, The Cryosphere, 6, 101–112, https://doi.org/10.5194/tc-6-101-2012, 2012.

Favier, L., Pattyn, F., Berger, S., and Drews, R.: Dynamic influence of pinning points on marine ice-sheet stability: a numerical study in Dronning Maud Land, East Antarctica, The Cryosphere, 10, 2623–2635, https://doi.org/10.5194/tc-10-2623-2016, 2016.

Gagliardini, O., Zwinger, T., Gillet-Chaulet, F., Durand, G., Favier, L., de Fleurian, B., Greve, R., Malinen, M., Martín, C., Råback, P., Ruokolainen, J., Sacchettini, M., Schäfer, M., Seddik, H., and Thies, J.: Capabilities and performance of Elmer/Ice, a new-generation ice sheet model, Geoscientific Model Development, 6, 1299–1318, https://doi.org/10.5194/gmd-6-1299-2013, 2013.

Gagliardini, O., Brondex, J., Gillet-Chaulet, F., Tavard, L., Peyaud, V., and Durand, G.: Brief communication: Impact of mesh resolution for MISMIP and MISMIP3d experiments using Elmer/Ice, The Cryosphere, 10, 307–312, https://doi.org/10.5194/tc-10-307-2016, 2016.

Gillet-Chaulet, F. and Hindmarsh, R. C.: Flow at ice-divide triple junctions: 1. Three-dimensional full-Stokes modeling, Journal of Geophysical Research: Earth Surface, 116, 2011.

Goel, V., Matsuoka, K., Berger, C. D., Lee, I., Dall, J., and Forsberg, R.: Characteristics of ice rises and ice rumples in Dronning Maud Land and Enderby Land, Antarctica, Journal of Glaciology, 66, 1064–1078, https://doi.org/10.1017/jog.2020.77, 2020.

Goldberg, D., Holland, D. M., and Schoof, C.: Grounding line movement and ice shelf buttressing in marine ice sheets, Journal of Geophysical Research, 114, F04 026, https://doi.org/10.1029/2008JF001227, 2009.

Greve, R. and Blatter, H.: Dynamics of ice sheets and glaciers, Springer, Dordrecht, 2009.

Gudmundsson, G. H., Krug, J., Durand, G., Favier, L., and Gagliardini, O.: The stability of grounding lines on retrograde slopes, The Cryosphere, 6, 1497–1505, https://doi.org/10.5194/tc-6-1497-2012, 2012.

Haseloff, M. and Sergienko, O. V.: The effect of buttressing on grounding line dynamics, Journal of Glaciology, 64, 417–431, https://doi.org/10.1017/jog.2018.30, 2018.

Hindmarsh, R. C., King, E. C., Mulvaney, R., Corr, H. F., Hiess, G., and Gillet-Chaulet, F.: Flow at ice-divide triple junctions: 2. Three-dimensional views of isochrone architecture from ice-penetrating radar surveys, Journal of Geophysical Research: Earth Surface, 116, 2011.

Hutter, K.: Theoretical glaciology: material science of ice and the mechanics of glaciers and ice sheets, Dordrecht, D. Reidel Publishing Co./Tokyo, Terra Scientific Publishing Co., 1983.

Jezek, K. C.: Observing the Antarctic Ice Sheet Using the RADARSAT-1 Synthetic Aperture Radar, Polar Geography, 27, 197–209, https://doi.org/10.1080/789610167, 2003.

Kingslake, J., Martín, C., Arthern, R. J., Corr, H. F. J., and King, E. C.: Ice-flow reorganization in West Antarctica 2.5 kyr ago dated using radar-derived englacial flow velocities, Geophysical Research Letters, 43, 9103–9112, https://doi.org/https://doi.org/10.1002/2016GL070278, 2016.

Kingslake, J., Scherer, R. P., Albrecht, T., Coenen, J., Powell, R. D., Reese, R., Stansell, N. D., Tulaczyk, S., Wearing, M. G., and Whitehouse, P. L.: Extensive retreat and re-advance of the West Antarctic Ice Sheet during the Holocene, Nature, 558, 430–434, https://doi.org/10.1038/s41586-018-0208-x, 2018.

Martín, C., Hindmarsh, R. C. A., and Navarro, F. J.: Dating ice flow change near the flow divide at Roosevelt Island, Antarctica, by using a thermomechanical model to predict radar stratigraphy, Journal of Geophysical Research, 111, F01 011, https://doi.org/10.1029/2005JF000326, 2006.

Martín, C., Hindmarsh, R. C. A., and Navarro, F. J.: On the effects of divide migration, along-ridge flow, and basal sliding on isochrones near an ice divide, Journal of Geophysical Research, 114, F02 006, https://doi.org/10.1029/2008JF001025, 2009.

Matsuoka, K., Hindmarsh, R. C., Moholdt, G., Bentley, M. J., Pritchard, H. D., Brown, J., Conway, H., Drews, R., Durand, G., Goldberg, D., Hattermann, T., Kingslake, J., Lenaerts, J. T., Martín, C., Mulvaney, R., Nicholls, K. W., Pattyn, F., Ross, N., Scambos, T., and Whitehouse, P. L.: Antarctic ice rises and rumples: Their properties and significance for ice-sheet dynamics and evolution, Earth-Science Reviews, 150, 724–745, https://doi.org/10.1016/j.earscirev.2015.09.004, 2015.

Pattyn, F., Schoof, C., Perichon, L., Hindmarsh, R. C. A., Bueler, E., de Fleurian, B., Durand, G., Gagliardini, O., Gladstone, R., Goldberg, D., Gudmundsson, G. H., Huybrechts, P., Lee, V., Nick, F. M., Payne, A. J., Pollard, D., Rybak, O., Saito, F., and Vieli, A.: Results of the Marine Ice Sheet Model Intercomparison Project, MISMIP, The Cryosphere, 6, 573–588, https://doi.org/10.5194/tc-6-573-2012, 2012.

Pattyn, F., Perichon, L., Durand, G., Favier, L., Gagliardini, O., Hindmarsh, R. C., Zwinger, T., Albrecht, T., Cornford, S., Docquier, D., Fürst, J. J., Goldberg, D., Gudmundsson, G. H., Humbert, A., Hütten, M., Huybrechts, P., Jouvet, G., Kleiner, T., Larour, E., Martin, D., Morlighem, M., Payne, A. J., Pollard, D., Rückamp, M., Rybak, O., Seroussi, H., Thoma, M., and Wilkens, N.: Grounding-line migration in plan-view marine ice-sheet models: results of the ice2sea MISMIP3d intercomparison, Journal of Glaciology, 59, 410–422, https://doi.org/10.3189/2013JoG12J129, 2013.

Pettit, E. C., Jacobson, H. P., and Waddington, E. D.: Effects of basal sliding on isochrones and flow near an ice divide, Annals of Glaciology, 37, 370–376, https://doi.org/10.3189/172756403781815997, 2003.

Pollard, D., Chang, W., Haran, M., Applegate, P., and DeConto, R.: Large ensemble modeling of the last deglacial retreat of the West Antarctic Ice Sheet: comparison of simple and advanced statistical techniques, Geoscientific Model Development, 9, 1697–1723, https://doi.org/10.5194/gmd-9-1697-2016, 2016.

Raymond, C. F.: Deformation in the Vicinity of Ice Divides, Journal of Glaciology, 29, 357–373, https://doi.org/10.1017/S0022143000030288, 1983.

Reese, R., Gudmundsson, G. H., Levermann, A., and Winkelmann, R.: The far reach of ice-shelf thinning in Antarctica, Nature Climate Change, 8, 53–57, https://doi.org/10.1038/s41558-017-0020-x, 2018.

Schannwell, C., Drews, R., Ehlers, T. A., Eisen, O., Mayer, C., and Gillet-Chaulet, F.: Kinematic response of ice-rise divides to changes in ocean and atmosphere forcing, The Cryosphere, 13, 2673–2691, https://doi.org/10.5194/tc-13-2673-2019, 2019.

Schannwell, C., Drews, R., Ehlers, T. A., Eisen, O., Mayer, C., Malinen, M., Smith, E. C., and Eisermann, H.: Quantifying the effect of ocean bed properties on ice sheet geometry over 40 000 years with a full-Stokes model, The Cryosphere, 14, 3917–3934, https://doi.org/10.5194/tc-14-3917-2020, 2020.

Schoof, C.: Ice sheet grounding line dynamics: Steady states, stability, and hysteresis, Journal of Geophysical Research, 112, F03S28, https://doi.org/10.1029/2006JF000664, 2007.

Sergienko, O. V. and Wingham, D. J.: Bed topography and marine ice-sheet stability, Journal of Glaciology, 68, 124–138, https://doi.org/10.1017/jog.2021.79, 2022.

Seroussi, H., Nowicki, S., Simon, E., Abe-Ouchi, A., Albrecht, T., Brondex, J., Cornford, S., Dumas, C., Gillet-Chaulet, F., Goelzer, H., Golledge, N. R., Gregory, J. M., Greve, R., Hoffman, M. J., Humbert, A., Huybrechts, P., Kleiner, T., Larour, E., Leguy, G., Lipscomb, W. H., Lowry, D., Mengel, M., Morlighem, M., Pattyn, F., Payne, A. J., Pollard, D., Price, S. F., Quiquet, A., Reerink, T. J., Reese, R., Rodehacke, C. B., Schlegel, N.-J., Shepherd, A., Sun, S., Sutter, J., Van Breedam, J., van de Wal, R. S. W., Winkelmann, R., and Zhang, T.: initMIP-Antarctica: an ice sheet model initialization experiment of ISMIP6, The Cryosphere, 13, 1441–1471, https://doi.org/10.5194/tc-13-1441-2019, 2019.

Smith, E. C., Smith, A. M., White, R. S., Brisbourne, A. M., and Pritchard, H. D.: Mapping the ice-bed interface characteristics of Rutford Ice Stream, West Antarctica, using microseismicity: Mapping ICE-Bed Interface, Rutford, Journal of Geophysical Research: Earth Surface, 120, 1881–1894, https://doi.org/10.1002/2015JF003587, 2015.

Still, H. and Hulbe, C.: Mechanics and dynamics of pinning points on the Shirase Coast, West Antarctica, The Cryosphere, 15, 2647–2665, https://doi.org/10.5194/tc-15-2647-2021, 2021.

Still, H., Campbell, A., and Hulbe, C.: Mechanical analysis of pinning points in the Ross Ice Shelf, Antarctica, Annals of Glaciology, 60, 32–41, https://doi.org/10.1017/aog.2018.31, 2019.

Vialov, S.: Regularities of glacial shields movement and the theory of plastic viscous flow, Physics of the Movements of Ice IAHS, 47, 266–275, 1958.

Wearing, M. G. and Kingslake, J.: Holocene Formation of Henry Ice Rise, West Antarctica, Inferred From Ice-Penetrating Radar, Journal of Geophysical Research: Earth Surface, 124, 2224–2240, https://doi.org/10.1029/2018JF004988, 2019.